Supporting Information

A Crystalline 2D Fullerene-based Metal Halide Semiconductor for Efficient and Stable Ideal-bandgap Perovskite Solar Cells

Weicheng Shen[1,2,#], Ali Azmy[3,#], Guang Li,[1,2,#] Anamika Mishra,[3] Zois Syrgiannis,[4] Wenwen Zheng,[1,*] George Volonakis,[5] Mikaël Kepenekian,[5] Jacky Even,[6] Lukasz Wojtas,[3] Cheng Wang,[2] Lishuai Huang,[2] Weiqing Chen,[2] Shun Zhou,[2] Jin Zhou,[2] Guojun Zeng,[2] Dexin Pu,[2] Hongling Guan,[2] Guojia Fang,[2] Weijun Ke,[2] and Ioannis Spanopoulos[3,*]

[1]*Hubei Key Laboratory of Optical Information and Pattern Recognition, School of Optical Information and Energy Engineering, Wuhan Institute of Technology, Wuhan 430205, China*
[2]*Key Lab of Artificial Micro- and Nano-Structures of Ministry of Education, School of Physics and Technology, Wuhan University, Wuhan 430072, China*
[3]*Department of Chemistry, University of South Florida, Tampa, FL, 33620, USA*
[4]*Nanoneurosciences LLC, 16192 Coastal HWY, Lewes, De, 19958, USA*
[5]*Univ Rennes, ENSCR, CNRS, ISCR-UMR 6226, F-35000 Rennes, France*
[6]*Univ Rennes, INSA Rennes, CNRS, Institut FOTON-UMR6082, F-35000 Rennes, France*

Corresponding Authors:
spanopoulos@usf.edu
wenwenzheng@wit.edu.cn

Table of contents

1. Materials and methods

Starting materials

All starting materials for synthesis were purchased commercially and were used without further purification. PbI_2 (99.99%), SnI_2 (99.99%), MAI (99.9%), FAI (99.9%), PEDOT: PSS was bought from Advanced Election Technology Co, Ltd. Glycine hydrochloride (GlyHCl) was obtained from Shanghai Aladdin Biochemical Technology Co. N,N-dimethylformamide (DMF, anhydrous, 99.8%), SnF_2 (98%), dichloromethane, and dimethyl sulfoxide (DMSO, anhydrous, 99.9%), chlorobenzene (CB, anhydrous, 99.8%), Hydriodic acid 57 wt. % in H_2O, distilled, stabilized, 99.95%, were purchased from Sigma-Aldrich. C_{60} (99.9%) and BCP (99.99%) were bought from Xi'an Polymer Light Technology (China). C_{60} (99%) was purchased from TCI, N-Boc-aminoethanol, pyridine, malonyl dichloride, CBr_4, DBU, $CDCl_3$, DMSO-d_6 (99.5%) were purchased from Fisher.

Preparation of precursor solutions

To prepare 1.8 M ideal bandgap $FA_{0.6}MA_{0.4}Pb_{0.7}Sn_{0.3}I_3$ precursors, SnI_2 (201.2 mg), PbI_2 (580.9 mg), FAI (185.7 mg), MAI (114.5 mg), MACl (8.5 mg), GlyHCl (2.04 mg), and Snf_2 (12.7 mg) was dissolved in 1 mL of DMF/DMSO solvent mixture (3:1 volume ratio) and stirred for 1 hour before use. The perovskite precursors were prepared in an N_2-filled glovebox and filtered with 0.22 μm polytetrafluoroethylene (PTFE) before use.

Device fabrication

The etched ITO substrates were sequentially cleaned with detergent, deionized water, acetone, and ethanol for 15 min each. Before spin-coating, the ITO substrates needed to be exposed to ultraviolet-ozone for 15 min. Then, PEDOT: PSS was spin-coated onto the ITO substrate at 5,000 rpm for 30 s and annealed at 140 °C for 25 min in ambient air. After annealing, the PEDOT: PSS-coated ITO substrates were immediately transferred to an N_2-filled glovebox with controlled H_2O and O_2 levels (both of them＜0.01 ppm). Next, the prepared perovskite precursor solution was spin-coated on the substrate at 1,000 rpm for 10 s and then spun at 4,500 rpm for 40 s. A 200 μL CB drop was applied to the spinning substrate after the beginning of 35 s. After completion of the spin-coating process, the obtained perovskite films were annealed on a hot bench at 110°C for 15 min. In addition, our target devices also needed to be post-treated with C_{60}-$2NH_3$. We dropped 0.75 mg/ml of C_{60}-$2NH_3$ (dissolved in CB) onto the annealed perovskite films, and then let the rotating substrate rotate at 5,000 rpm for 30 s, next annealed the perovskite films on the hot bench at 100°C for 5 min after the rotation. Finally, C_{60} (20 nm), BCP (7 nm), and Cu (100 nm) were sequentially deposited on the prepared perovskite films, and the solar cells were completed by thermal evaporation under a high-vacuum system (< 5 × 10-4 Pa).

Film characterization

TA tests in this study used a pump beam with a center wavelength of 360 nm and a pulse energy density of 1.2 μJ / cm^2 to produce a probe beam of 350-750 nm in a Harpia spectrometer. XPS measurements were conducted with a monochromatic Al-Kα X-ray source by an XPS/UPS system (Thermo Scientific, ESCLAB 250Xi). UPS spectra were conducted in the same system with a He I UV source at a bias voltage of -10 V. Top-view and cross-section images of perovskite films and devices were obtained using a Zeiss SIGMA field emission SEM. The surface roughness of the films was characterized by a Bruker Dimension Icon XR AFM. Crystal structure and phase of the films were characterized by XRD using a Cu Kα radiation source (Bruker, D8 ADVANCE). Absorption spectra were measured by a UV-visible spectrophotometer (SHIMADZU, mini 1280).

Device characterization

Photovoltaic parameters were obtained using a Keithley 2400 source meter under standard AM 1.5 G illumination (100 mW cm^{-2}) produced by a solar simulator (Enlitech, SS-F5-3A). The solar simulator was calibrated to a 100 mW cm^{-2} light intensity by a silicon reference solar cell. *J-V* measurements were performed by scanning from -0.1 to 1.0 V and then reversed again from 1.0 to -0.1 V with a voltage step of 20 mV and a delay time of 25 ms. Dark *J-V* measurements were conducted under dark conditions with bias voltages ranging from -0.4 V to 1 V. Light intensity dependence measurements were taken by decreasing the intensity of solar irradiation. SPO efficiencies were obtained by tracking the maximum power points. All the devices were measured for *J–V* curves by masking the active area (0.0948 cm^2) with a metal mask (the certified area is 0.070225 cm^2) in an N_2-filled glovebox. EQE measurements were carried out with a QE system (Enli Technology Co., Ltd) calibrated by a standard silicon cell. EIS and Mott–Schottky plots were recorded by a CHI760E electrochemical workstation (Shanghai Chenhua Instruments). Mott– Schottky measurements were conducted at 1 kHz with bias voltages ranging from 1.4 to 0 V in dark conditions. EIS measurements were recorded with a bias voltage of 0 V and a frequency range of 1 MHz ~ 1 Hz in dark conditions.

XRD measurements

Single-crystal X-ray diffraction

X-ray diffraction data were measured on a Bruker D8 Venture PHOTON II CMOS diffractometer equipped with a Cu Kα INCOATEC ImuS micro-focus source (λ = 1.54178 Å) equipped with a cryostream 800 system (Oxford Cryosystems) for temperature regulation. Indexing was performed using APEX4 (Difference Vectors method).[1] Data integration and reduction were performed using SaintPlus.[2] Absorption correction was performed by a multi-scan method implemented in SADABS.[3] Space group was determined using XPREP implemented in APEX3. Structure was solved using SHELXT[4] and refined using SHELXL-2018/3 (full-matrix least-squares on F2)[5] through OLEX2 interface program.[6] Ellipsoid plot was done with Platon.[7] Disordered molecule was refined with restraints. All hydrogen atoms were located geometrically and were refined using a riding model.

Powder X-ray diffraction

Powder X-ray diffraction patterns were collected on a Bruker D8 Advance Diffractometer with a Lynxeye detector using CuKα radiation. X-ray source operated at 40kV/40mA and Ni filter was used to suppress Kbeta radiation. 2.5 deg primary and secondary Soller slits were used to suppress axial divergence. Diffraction patterns were recorded from 2 to 60 2θ in variable slits mode and with knife edge installed. A typical scan rate was 20 sec/step with a step size of 0.02 deg.

Optical Spectroscopy

Optical diffuse-reflectance measurements were performed at room temperature using a Cary 5000 UV-Vis-NIR Spectrophotometer, coupled with an integrating sphere, from 200 to 2500 nm. $BaSO_4$ was used as a non-absorbing reflectance reference. The generated reflectance-versus-wavelength data were used to estimate the band gap of the material by converting reflectance to absorbance data according to the Kubelka−Munk equation: $\alpha/S = (1 - R)^2/2R$, where R is the reflectance and α and S are the absorption and scattering coefficients, respectively.[8]

Conductivity measurements

For the assessment of film conductivity, films both with and without C_{60}-$2NH_3$ were spin-coated onto ITO substrates, followed by the evaporation of metal electrodes. Subsequently, *I-V* curves of the devices were measured using an electrochemical workstation to obtain the resistance of the films. The resistivity was then calculated to determine the electrical conductivity.

DFT Studies

First-principles calculations are based on density functional theory (DFT) as implemented in the SIESTA package.[9-10] The nonlocal van der Waals density functional of Dion et al. corrected by Cooper (C09) is used for geometry optimizations,[11-12] while subsequent single-point calculations are performed using the revPBE functional[13] including spin-orbit coupling through the so-called off-site approach following the Hemstreet formalism.[14] Core electrons are described with Troullier-Martins pseudopotentials,[15] while valence wavefunctions are developed over a double-ζ polarized basis set of finite-range numerical pseudoatomic orbitals.[16] An energy cutoff of 150 Ry for real-space mesh size has been used. The Brillouin zone is sampled using a using a 7×7×2 Γ-centered Monkhorst-Pack grid. The experimental structure of $(C_{60}\text{-}2NH_3)Pb_2I_6$ is used for the inorganic skeleton, well characterized by X-ray diffraction. On the other hand, the positions of light atoms, more difficult to grasp experimentally, are optimized using the non-local van der Waals functional of Dion et al. corrected by Cooper (C09).[11-12]

In Figure 3, the revPBE gaps are corrected by applying a rigid shift to the conduction bands taken from the variation of bandgaps obtained going from PBE to HSE06 functional (Table S6). All HSE06 hybrid functional calculations reported in the manuscript were performed using the VASP code.[17] We employed a 2x2x1 Γ-centered k-point grid and an energy cut-off of 400 eV for the PAW pseudopotentials.[18] For all calculations we included spin-orbit coupling (SOC) interactions.

In order to highlight the composite nature of $(C_{60}\text{-}2NH_3)Pb_2I_6$, we consider the band structures of the inorganic and organic subsystems, $[Pb_2I_6]^{2-}$ and $[C_{60}\text{-}2NH_3]^{2+}$. To describe those systems in charge-balanced simulation cells, we substitute, first, the organic cations by Cs^+ ions placed at the position of N atoms. In the second case, only the organic moiety is conserved and N atoms are substituted by C atoms.

In addition, we provide high-frequency dielectric constant profiles along the stacking direction following the recipe detailed thoroughly in previous studies.[19-20]

Organic Synthesis

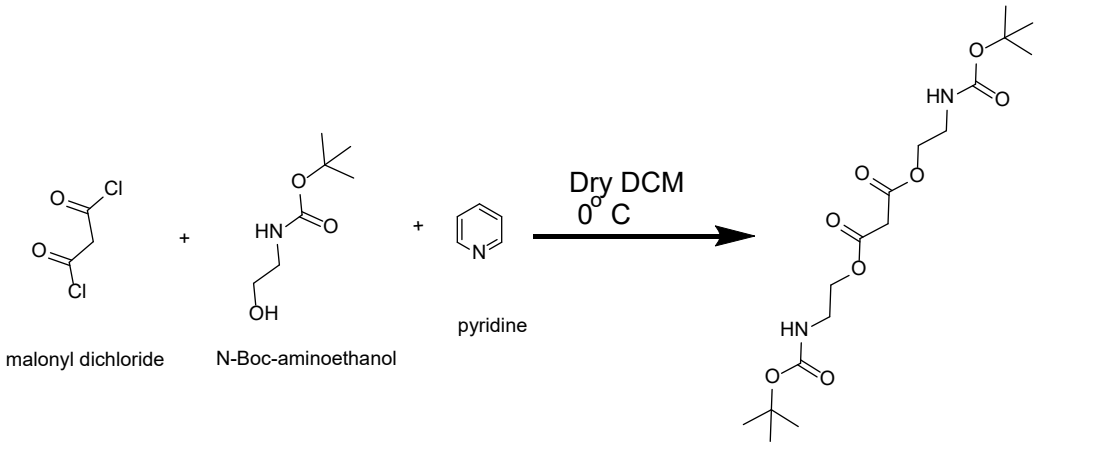

Scheme S1. The synthesis of the functionalized malonate ester (Compound **1**).

Synthesis of 1: In a round-bottomed flask, N-Boc-aminoethanol (5.00 g, 31.02 mmol, 2.2 mole equivalent) was dissolved in dry dichloromethane (300 mL) in an inert atmosphere. Pyridine (1.71 mL, 21.17 mmol, 1.5 mole equivalent) was added to the solution and the reaction mixture was cooled in an ice bath. Thereafter, a solution of malonyl dichloride (1.37 mL, 14.12 mmol, 1.0 mole equivalent) in dry dichloromethane (125 mL) was added dropwise over a period of 1.5 hours. The reaction mixture was further stirred for 2 hours at 0 °C and room temperature for 10 hours. It was then washed with saturated aqueous solution of ammonium chloride and water followed by drying over $MgSO_4$. Finally, the organic layer was recovered under vacuum and purification was performed by column chromatography on silica gel using a mixture of hexane/ethyl acetate (3:2, v:v). On evaporation of the solvent in a vacuum, the desired product was obtained as colorless oil which turns white solid (4.32 g, yield 78 %) on standing at room temperature 22 °C.

^{1}H-NMR ($CDCl_3$, 600 MHz, RT): δ = 4.95 (br, 2H, NH), 4.22 (t, 3 J = 5.2 Hz, 4H, OCH_2), 3.42 (m, 4H, CH_2NH), 3.40 (s, 2H, $O_2CCH_2CO_2$), 1.44 (s, 18H, $C(CH_3)_3$) ppm.

^{13}C-NMR ($CDCl_3$, 250 MHz, RT): δ = 166.46 (2C, C=O), 155.86 (2C, CONH), 79.60 (2C, $C(CH_3)_3$), 64.74 (2C, OCH_2), 41.21 (1C, $O_2CCH_2CO_2$), 39.34 (2C, CH_2NH), 28.24 (6C, $C(CH_3)_3$) ppm.

Sample Preparation: 1 mg compound was dissolved in 1 mL ethanol to make a clear solution. It was filtered and an LCMS experiment was performed. Observed MS (LC-MS) m/z: [M-H]+: Calculated for $C_{17}H_{30}N_2O_8$:389.43; Found: 389.20.

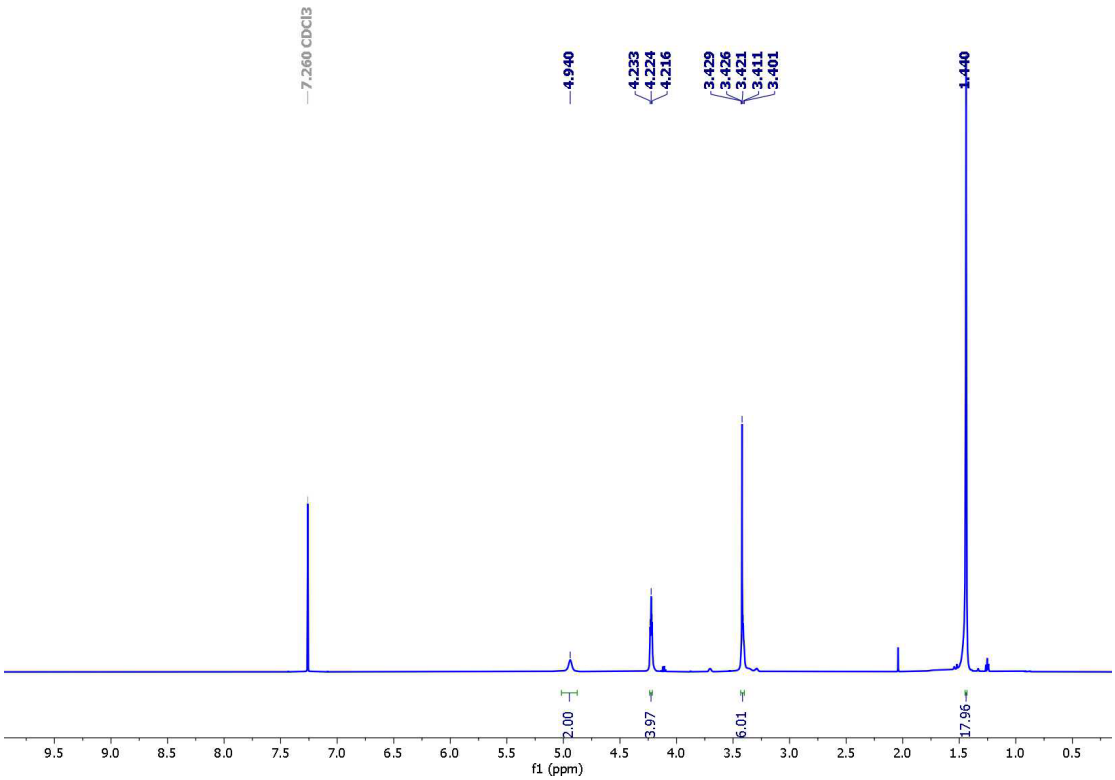

Figure S1. ^{1}H-NMR spectrum of compound **1** in $CDCl_3$. The peak at 2 ppm is due to residual ethyl acetate.

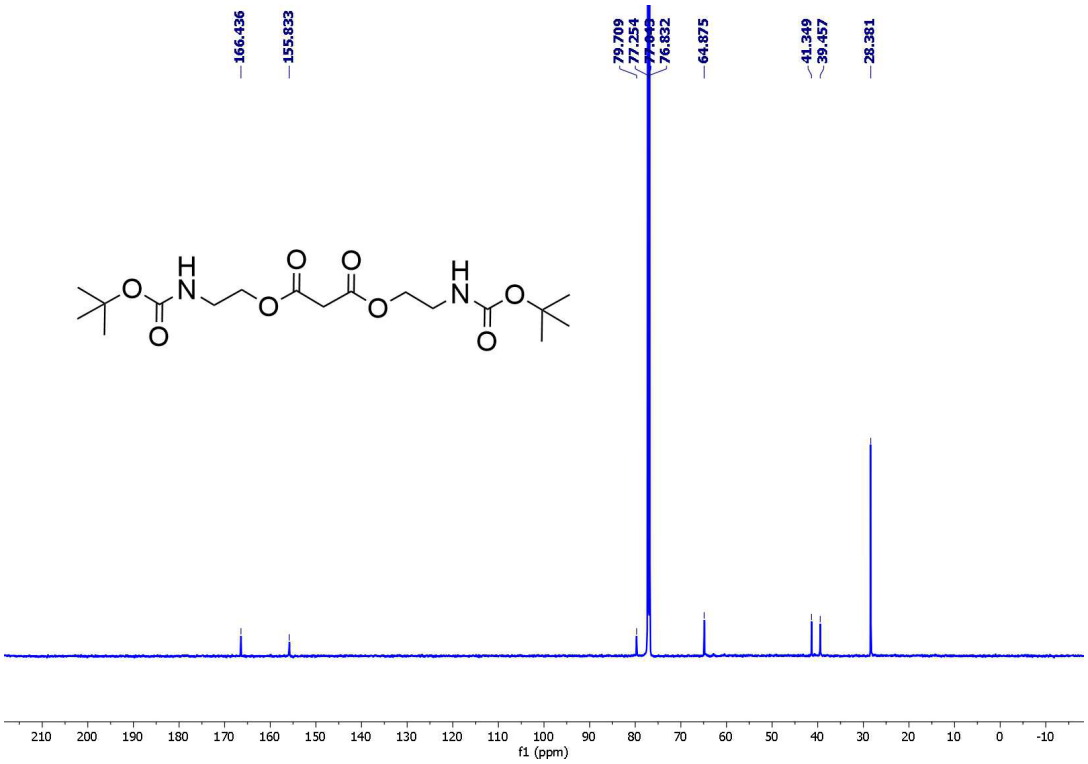

Figure S2. ^{13}C-NMR spectrum of compound **1** in $CDCl_3$.

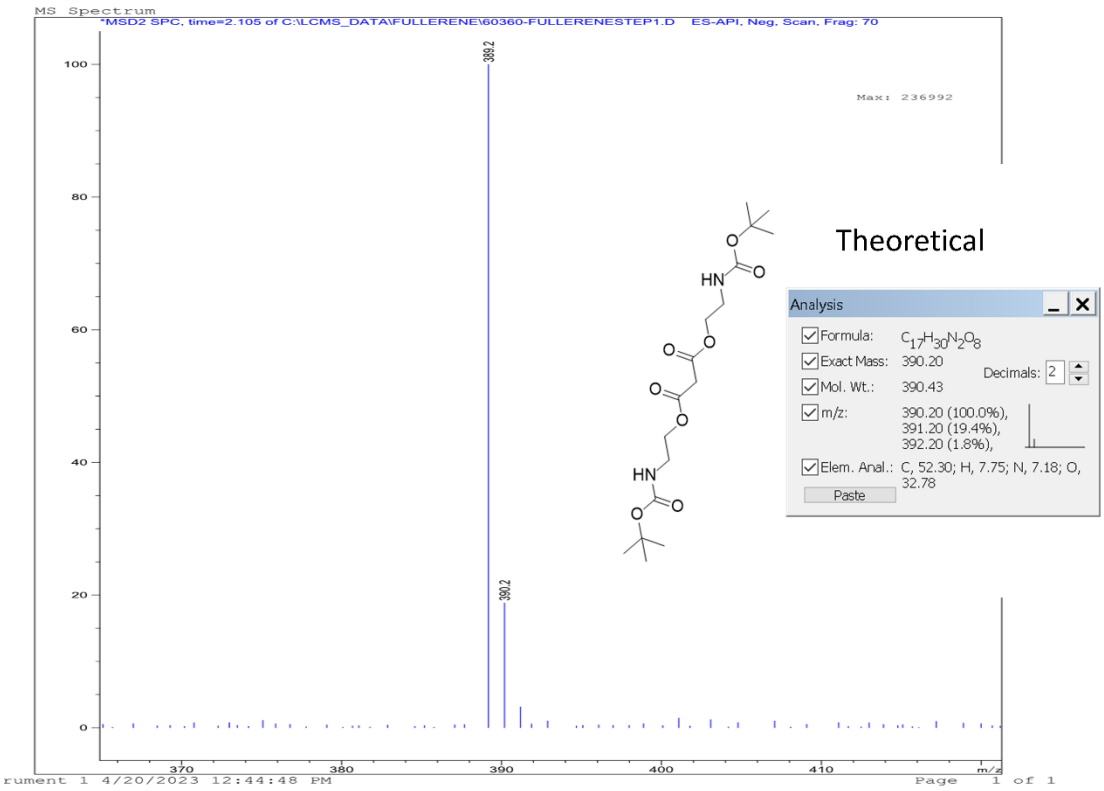

Figure S3. LC-MS spectrum of compound **1**.

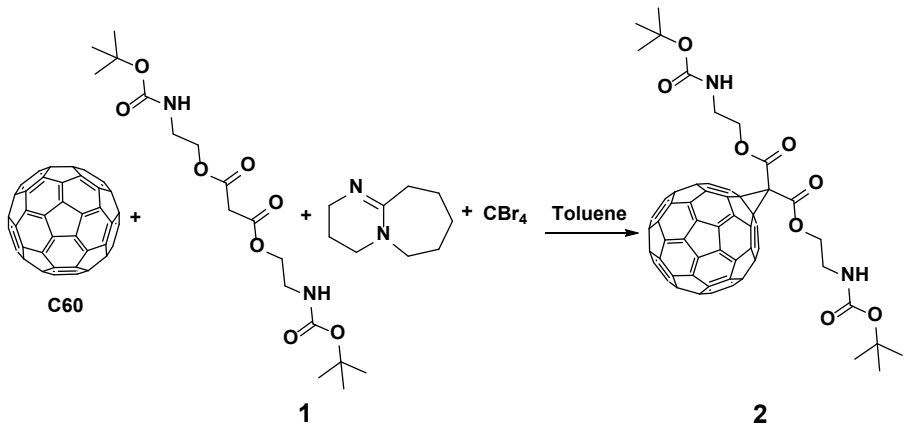

Scheme S2. The synthesis of the fullerene-malonate monoadduct (Compound **2**).

Synthesis of 2: In the dark, C_{60} (3g. 4.16 mmol, 1 mole equivalent) and CBr4 (2.07 g, 6.24 mmol, 1.5 mole equivalent) were dissolved in toluene (500 mL) at RT (22 ºC) by sonication. The solution was then cooled in an ice bath to maintain a temperature of 0-10 ºC while malonate **1** (2.44 g, 6.24 mmol, 1.5-mole equivalent) and DBU (1.85 mL, 1.89 g, 3 mmol, 3-mole equivalent) were added. On stirring at 10 ºC the reaction was complete after 2 hours (monitored with thin layer chromatography). The crude reaction mixture was purified by column chromatography on silica gel using toluene as eluent to remove unreacted C_{60}, followed by 10:1 toluene/ethyl acetate to yield, after evaporation and drying 1.80 g (39.13%) of the desired mono-adduct **2**.

^{1}H-NMR ($CDCl_3$, 600 MHz, RT): δ = 5.02 (br, 2H, NH), 4.52 (m, 4H, OCH_2), 3.55 (m, 4H, CH_2NH), 1.40 (s, 18H, $C(CH_3)_3$) ppm.

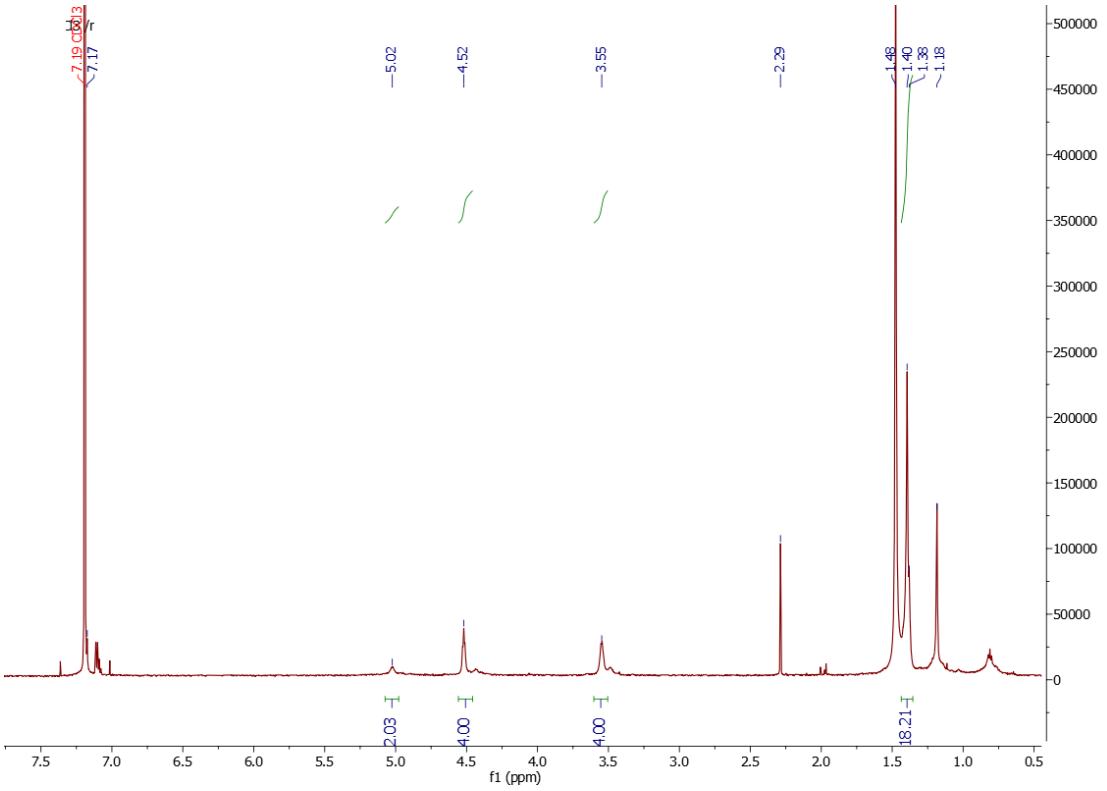

Figure S4. ^{1}H-NMR spectrum of compound **2** in $CDCl_3$. The peak at 2.29ppm corresponds to residual toluene, the peak at 1.48ppm corresponds to H_2O, while the peak at 1.18ppm corresponds to grease used for sealing glass connections.

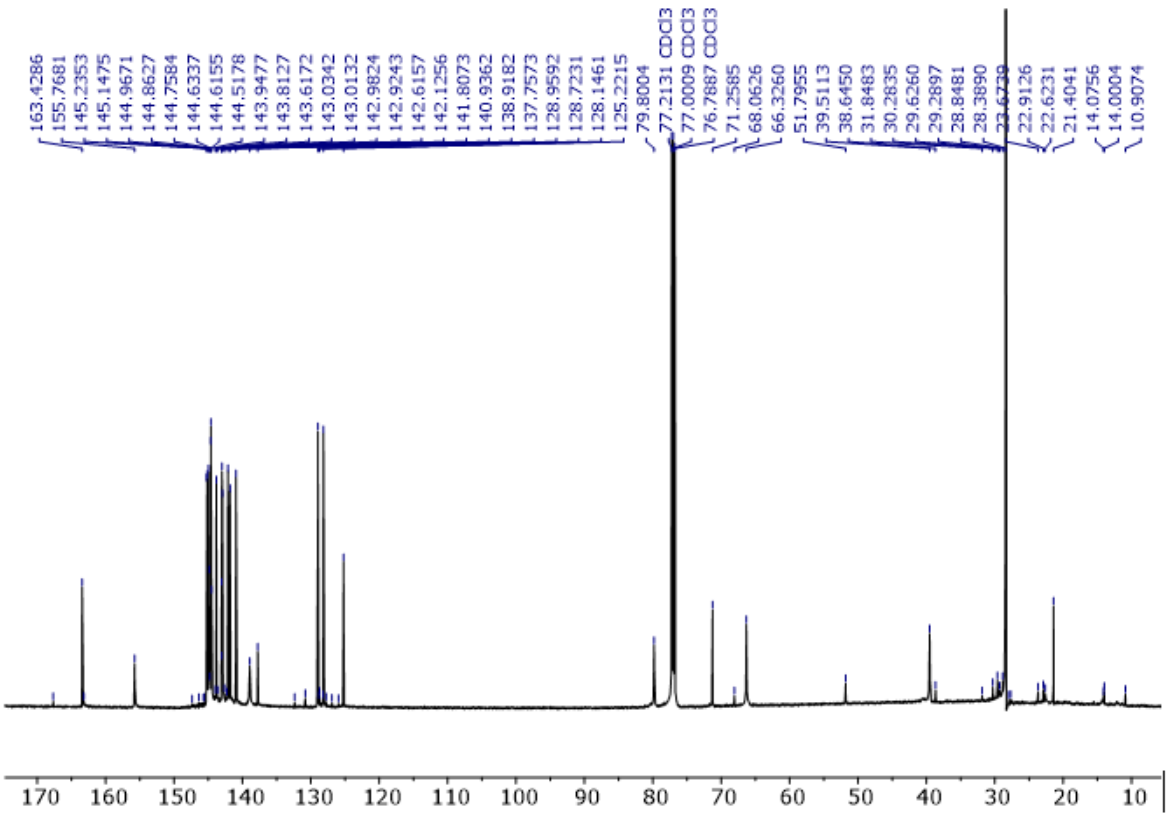

Figure S5. ^{13}C-NMR spectrum of compound **2** in $CDCl_3$.

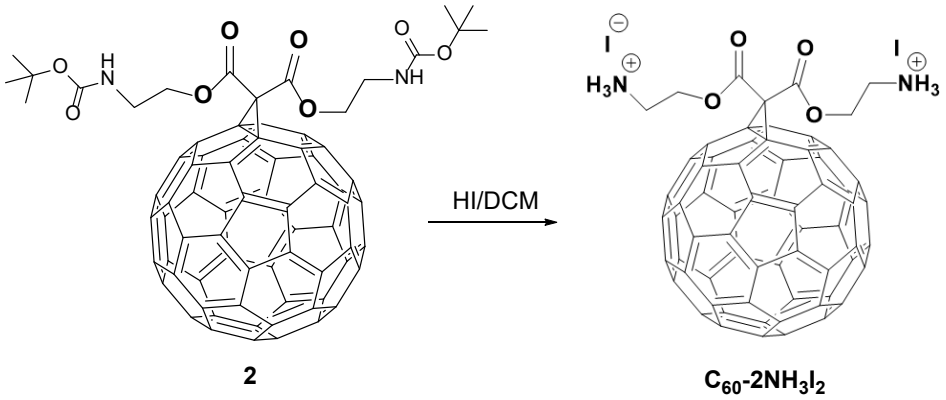

Scheme S3. The synthesis of the amino-functionalized fullerene derivative (C_{60}-$2NH_3I_2$).

Synthesis of C_{60}-$2NH_3I_2$: In a single neck round bottom flask (50 mL), compound **2** (1g) is dissolved in DCM (5 mL). The solution is purged with Ar. An aqueous solution of HI (57%, 4 mL) was added dropwise which changed the light brown color solution into a thick dark red mixture. The mixture was stirred at RT for 48 hours. The mixture was then centrifuged and washed with DCM 5 times (5 ml each time). The dark brown powder was formed which was dried for 4 days under vacuum (0.75 g, 73%).

^{1}H-NMR (DMSO-d_6, 600 MHz, RT): δ = 8.19 (t, 6H, NH_3), 4.72 (m, 4H, OCH_2), 3.40 (m, 4H, CH_2NH) ppm.

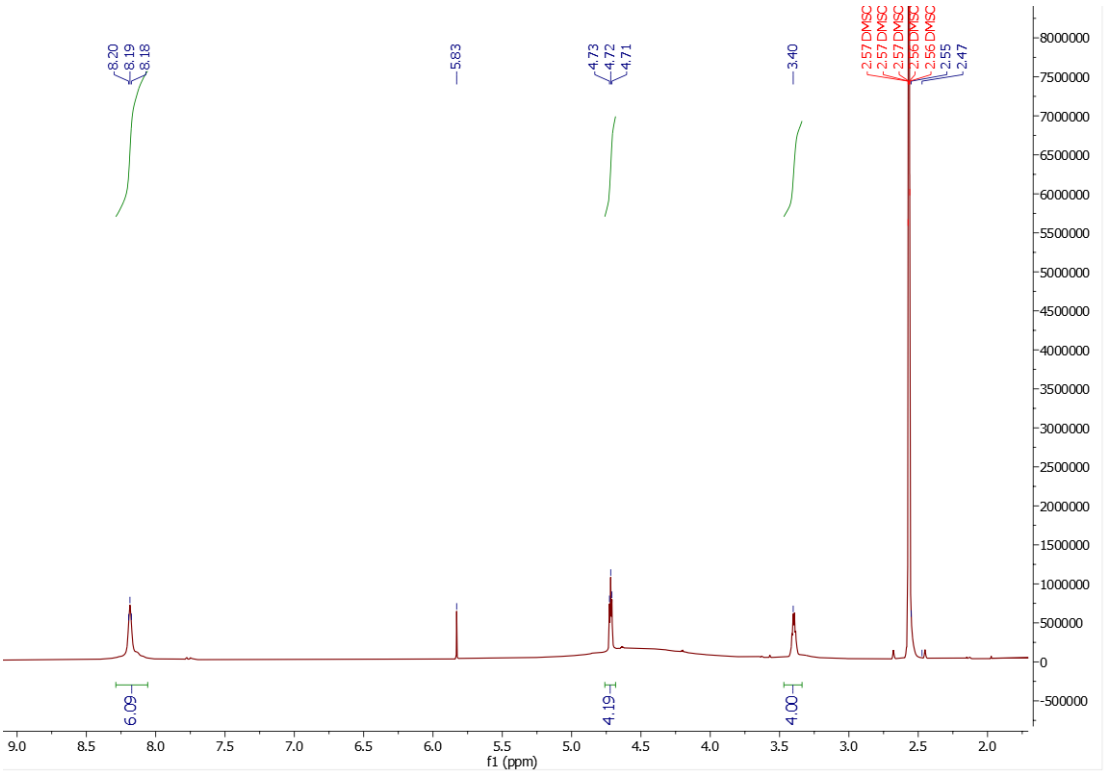

Figure S6. ^{1}H-NMR spectrum of **C_{60}-2NH_3I_2** in DMSO-d_6. The peak at 5.83 ppm is residual DCM.

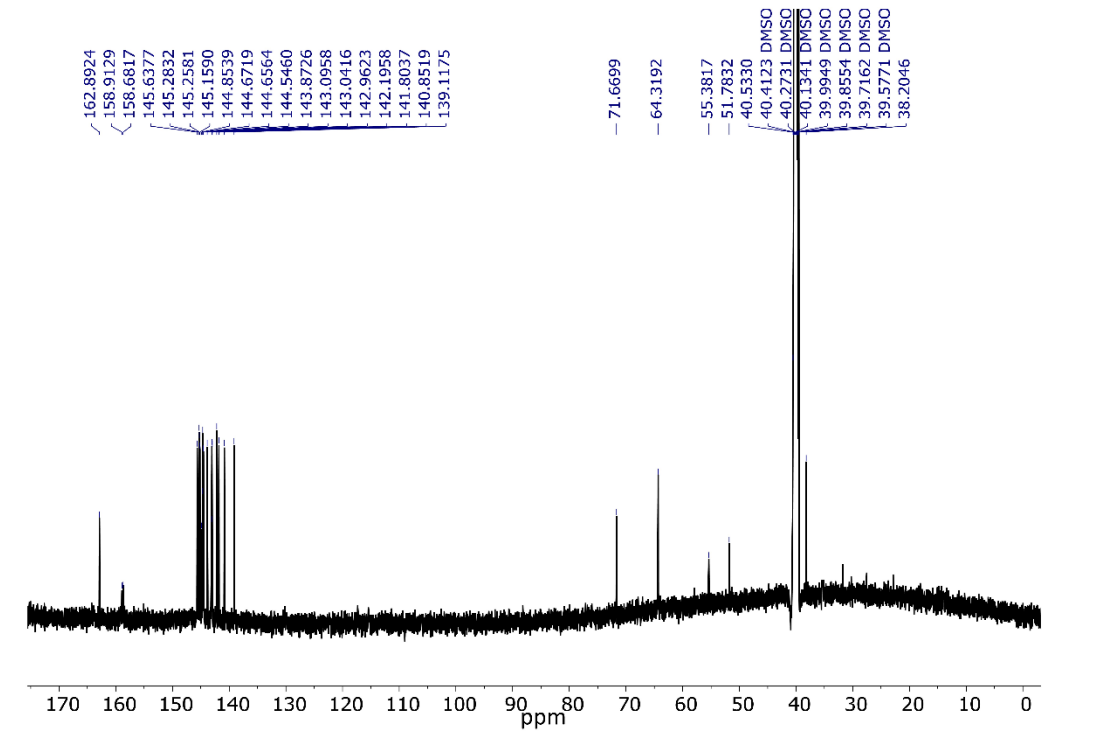

Figure S7. ^{13}C-NMR spectrum of **C_{60}-2NH_3I_2** in DMSO-d_6.

3. Material synthesis

(C_{60}-$2NH_3$)Pb_2I_6: 30mg (0.026mmol) of the C_{60}-$2NH_3I_2$ were dissolved in a solution consisting of 0.5mL of 99.8% Extra Dry DMF, by sonicating at RT for 5min. Then 24mg (0.052mmol) of PbI_2 was added to the solution and dissolved using sonication. The vial was placed uncapped in a larger vial containing 3mL of Dichloromethane. Finally, the larger container vial was capped and left at RT where brown crystals formed overnight. They were collected by suction filtration and dried under vacuum overnight.

4. Characterization

Table S1. Crystal data and structure refinement for $(C_{60}\text{-}2NH_3)Pb_2I_6$ at 296.15 K.

Empirical formula	C67 H14 I6 N2 O4 Pb2
Formula weight	2086.58
Temperature	296.15 K
Wavelength	1.54178 Å
Crystal system	triclinic
Space group	*P*-1
Unit cell dimensions	a = 10.0971(9) Å, α = 82.189(5)° b = 10.2000(9) Å, β = 85.406(5)° c = 31.287(3) Å, γ = 84.539(5)°
Volume	3170.5(5) $Å^3$
Z	2
Density (calculated)	2.186 g/cm^3
Absorption coefficient	33.521 mm^{-1}
F(000)	1888
Crystal size	0.07 x 0.06 x 0.02 mm^3
θ range for data collection	1.428 to 65.083°
Index ranges	-11<=h<=11, -11<=k<=11, -36<=l<=36
Reflections collected	103122
Independent reflections	10727 [R_{int} = 0.1240]
Completeness to θ = 65.083°	99.5%
Refinement method	Full-matrix least-squares on F^2
Data/restraints/parameters	10727 / 1978 / 731
Goodness-of-fit	1.469
Final R indices [I > 2σ(I)]	R_{obs} = 0.1245, wR_{obs} = 0.3363
R indices [all data]	R_{all} = 0.1385, wR_{all} = 0.3519

Largest diff. peak and hole	7.041 and -3.492 e·Å^{-3}

Table S2. Atomic coordinates ($x10^4$) and equivalent isotropic displacement parameters ($Å^2x10^3$) for $(C_{60}\text{-}2NH_3)Pb_2I_6$ at 296.15 K with estimated standard deviations in parentheses.

Label	**x**	**y**	**z**	**Occupancy**	**U_{eq}***
Pb(1)	-7574(2)	7454(2)	733(1)	1	57(1)
Pb(2)	-6729(2)	11749(1)	37(1)	1	53(1)
I(1)	-7977(4)	10412(2)	936(1)	1	104(2)
I(2)	-4511(2)	7264(3)	953(1)	1	72(1)
I(3)	-6387(2)	8807(2)	-282(1)	1	54(1)
I(4)	-6801(2)	4510(2)	396(1)	1	72(1)
I(5)	-10515(2)	7624(3)	370(2)	1	90(1)
I(6)	-8616(3)	6406(3)	1631(1)	1	96(1)
C(1)	-2390(40)	5320(40)	4587(16)	1	183(9)
C(2)	-3600(40)	4860(40)	4580(15)	1	178(9)
C(3)	-3660(40)	3400(40)	4619(15)	1	174(9)
C(4)	-2620(40)	2450(40)	4647(15)	1	172(9)
C(5)	-1270(40)	2990(40)	4648(13)	1	173(9)
C(6)	-1130(50)	4360(40)	4615(14)	1	174(9)
C(7)	-210(40)	5060(40)	4355(14)	1	172(9)
C(8)	700(50)	4340(40)	4082(13)	1	166(9)
C(9)	620(40)	2880(40)	4110(12)	1	159(9)
C(10)	-270(40)	2230(40)	4368(13)	1	171(9)
C(11)	-1110(40)	1170(40)	4250(12)	1	159(8)
C(12)	-2480(40)	1330(40)	4429(13)	1	166(8)
C(13)	-3420(40)	1070(50)	4193(11)	1	160(8)
C(14)	-4680(40)	2070(40)	4181(12)	1	159(8)
C(15)	-4790(50)	3050(40)	4381(14)	1	169(9)
C(16)	-5340(50)	4470(40)	4199(13)	1	164(8)
C(17)	-4500(50)	5470(40)	4333(15)	1	175(9)

C(18)	-4270(50)	6590(50)	4091(13)	1	180(9)
C(19)	-2910(40)	7190(50)	4045(13)	1	172(9)
C(20)	-2070(40)	6510(50)	4319(15)	1	178(9)
C(21)	-700(50)	6400(40)	4148(14)	1	170(9)
C(22)	-260(50)	6850(50)	3724(12)	1	168(9)
C(23)	-1190(40)	7470(40)	3414(13)	1	159(9)
C(24)	-2630(40)	7630(40)	3572(13)	1	163(9)
C(25)	-3710(40)	7420(40)	3335(12)	1	165(9)
C(26)	-4700(40)	6770(40)	3638(13)	1	166(9)
C(27)	-5420(40)	5820(40)	3490(13)	1	160(8)
C(28)	-5750(50)	4630(40)	3770(12)	1	156(8)
C(29)	-5590(40)	3470(40)	3542(12)	1	147(8)
C(30)	-5090(40)	2230(40)	3732(12)	1	146(8)
C(31)	-4200(40)	1490(50)	3500(11)	1	142(8)
C(32)	-3280(40)	900(50)	3802(11)	1	152(8)
C(33)	-1980(40)	800(40)	3598(11)	1	138(8)
C(34)	-810(40)	900(50)	3851(11)	1	149(8)
C(35)	250(40)	1490(40)	3581(11)	1	145(8)
C(36)	950(40)	2520(40)	3711(12)	1	151(8)
C(37)	1250(40)	3660(40)	3410(11)	1	153(8)
C(38)	1160(50)	4750(40)	3663(13)	1	161(8)
C(39)	700(50)	5970(40)	3470(13)	1	161(8)
C(40)	150(40)	6140(40)	3007(12)	1	150(8)
C(41)	-1010(40)	7140(50)	3010(13)	1	155(8)
C(42)	-2050(40)	7000(40)	2758(14)	1	148(8)
C(43)	-3400(40)	7060(40)	2946(13)	1	155(8)
C(44)	-4040(40)	6060(40)	2814(13)	1	143(8)

C(45)	-5090(40)	5470(40)	3068(13)	1	148(8)
C(46)	-5250(40)	4000(40)	3132(12)	1	140(8)
C(47)	-4370(30)	3320(40)	2853(11)	1	134(8)
C(48)	-3730(40)	2010(40)	3065(11)	1	135(8)
C(49)	-2450(40)	1810(40)	2897(10)	1	124(7)
C(50)	-1520(40)	1220(40)	3162(10)	1	125(8)
C(51)	-160(40)	1710(40)	3115(11)	1	134(7)
C(52)	120(40)	2830(40)	2854(12)	1	133(7)
C(53)	810(40)	3800(40)	3005(11)	1	137(8)
C(54)	260(40)	5090(40)	2816(12)	1	135(8)
C(55)	-710(30)	4890(30)	2555(12)	1	124(7)
C(56)	-1850(40)	5790(40)	2522(14)	1	132(7)
C(57)	-3100(40)	5160(40)	2534(12)	1	135(8)
C(58)	-3340(30)	3880(30)	2549(10)	1	119(7)
C(59)	-2200(30)	2900(30)	2546(10)	1	111(6)
C(60)	-710(30)	3440(30)	2530(10)	1	114(6)
C(61)	-1260(40)	2840(30)	2138(8)	1	103(6)
C(62)	-1410(40)	3560(40)	1710(9)	1	90(8)
O(63)	-2070(30)	4630(30)	1643(9)	1	96(8)
O(64)	-690(30)	3170(30)	1405(7)	1	82(6)
C(65)	-480(50)	3980(40)	988(9)	1	91(7)
H(65A)	-598.33	4905.25	1031.81	1	110
H(65B)	438.37	3794.96	879.54	1	110
C(66)	-1330(50)	3780(40)	666(12)	1	93(7)
H(66A)	-2222.61	4183.9	722.98	1	111
H(66B)	-985.55	4143.93	381	1	111
N(67)	-1320(50)	2380(30)	701(13)	1	110(8)

H(67A)	-1837.51	2168.34	507.34	1	132
H(67B)	-491.47	2028.9	650.75	1	132
H(67C)	-1629.77	2065.68	965.42	1	132
C(68)	-680(40)	1260(30)	2080(12)	1	96(7)
O(69)	480(40)	790(40)	2191(14)	1	127(12)
O(70)	-1460(40)	610(40)	1922(12)	1	120(9)
C(71)	-900(70)	-520(60)	1720(20)	1	163(17)
H(71A)	47.6	-447.24	1654.44	1	196
H(71B)	-994.91	-1319.08	1927.49	1	196
C(72)	-1500(60)	-660(90)	1340(20)	1	170(20)
H(72A)	-1317.76	-1577.75	1289.98	1	208
H(72B)	-1047.71	-123.77	1105.3	1	208
N(73)	-2910(50)	-330(50)	1308(17)	1	139(15)
H(73A)	-3136.52	-466.73	1049.09	1	167
H(73B)	-3364.83	-832.09	1512.75	1	167
H(73C)	-3112.87	524.49	1340.44	1	167

*U_{eq} is defined as one third of the trace of the orthogonalized U_{ij} tensor.

Table S3. Anisotropic displacement parameters ($Å^2x10^3$) for $(C_{60}\text{-}2NH_3)Pb_2I_6$ at 296.15 K with estimated standard deviations in parentheses.

Label	**U_{11}**	**U_{22}**	**U_{33}**	**U_{12}**	**U_{13}**	**U_{23}**
Pb(1)	54(1)	48(1)	69(1)	-8(1)	2(1)	-9(1)
Pb(2)	48(1)	41(1)	72(1)	-4(1)	0(1)	-12(1)
I(1)	163(3)	50(2)	97(2)	-18(2)	47(2)	-20(2)
I(2)	57(2)	80(2)	79(2)	-18(2)	-6(2)	-4(2)

I(3)	55(1)	45(1)	64(2)	-6(1)	-7(1)	-11(1)
I(4)	76(2)	46(1)	96(2)	-10(1)	5(2)	-24(2)
I(5)	52(2)	110(2)	110(2)	4(2)	-15(2)	-21(2)
I(6)	107(2)	97(2)	82(2)	-23(2)	20(2)	-6(2)
C(1)	195(14)	204(15)	154(18)	-42(11)	7(11)	-36(12)
C(2)	193(15)	205(15)	142(18)	-41(11)	9(12)	-38(11)
C(3)	189(15)	203(15)	135(19)	-38(11)	9(12)	-38(11)
C(4)	189(14)	202(15)	130(18)	-38(11)	7(10)	-41(12)
C(5)	192(15)	201(15)	133(17)	-42(11)	6(11)	-42(11)
C(6)	196(15)	202(15)	133(17)	-43(11)	3(12)	-43(11)
C(7)	195(15)	194(15)	135(15)	-43(11)	3(12)	-46(11)
C(8)	191(19)	193(14)	125(12)	-42(11)	-3(12)	-44(10)
C(9)	181(18)	192(15)	115(12)	-41(12)	-4(11)	-40(10)
C(10)	192(15)	201(16)	129(14)	-45(12)	5(11)	-42(11)
C(11)	181(14)	188(17)	112(12)	-36(11)	2(10)	-28(11)
C(12)	183(14)	199(17)	122(14)	-36(11)	4(10)	-35(12)
C(13)	177(14)	193(17)	113(11)	-33(11)	9(9)	-30(10)
C(14)	174(15)	191(15)	113(12)	-34(11)	15(10)	-29(10)
C(15)	183(16)	199(14)	129(15)	-34(11)	13(12)	-39(10)
C(16)	177(17)	196(15)	120(13)	-33(11)	22(12)	-39(10)
C(17)	191(16)	204(15)	135(15)	-39(11)	15(13)	-41(11)
C(18)	197(16)	207(17)	141(13)	-42(12)	14(11)	-40(11)
C(19)	192(15)	195(18)	136(13)	-36(12)	15(10)	-46(11)
C(20)	196(14)	202(16)	142(15)	-41(11)	10(11)	-39(12)
C(21)	193(15)	191(16)	136(13)	-44(11)	7(11)	-46(11)
C(22)	190(15)	184(17)	137(12)	-36(12)	8(10)	-48(10)
C(23)	183(14)	167(18)	136(12)	-40(11)	12(10)	-47(11)

C(24)	185(14)	170(20)	138(13)	-35(11)	14(10)	-47(11)
C(25)	178(15)	188(18)	136(12)	-36(12)	20(10)	-51(10)
C(26)	178(16)	191(17)	135(12)	-33(13)	22(10)	-48(10)
C(27)	172(18)	185(14)	126(12)	-30(12)	23(10)	-39(10)
C(28)	164(19)	185(14)	121(12)	-30(11)	24(10)	-38(10)
C(29)	154(18)	179(13)	109(11)	-29(10)	22(10)	-31(9)
C(30)	153(15)	177(14)	111(11)	-36(11)	21(9)	-27(10)
C(31)	154(13)	170(16)	102(10)	-35(11)	19(8)	-20(9)
C(32)	168(13)	178(19)	111(11)	-28(11)	8(9)	-24(10)
C(33)	165(12)	150(20)	102(10)	-27(10)	3(8)	-21(10)
C(34)	170(14)	169(19)	112(11)	-29(12)	-2(9)	-24(10)
C(35)	168(14)	167(16)	105(11)	-29(12)	-8(9)	-26(9)
C(36)	169(18)	179(14)	113(11)	-34(12)	-7(10)	-34(9)
C(37)	176(19)	178(14)	115(11)	-34(11)	-8(10)	-37(9)
C(38)	184(19)	183(13)	126(12)	-39(11)	-4(10)	-45(9)
C(39)	181(16)	182(14)	129(12)	-38(11)	2(10)	-46(10)
C(40)	165(16)	167(13)	128(13)	-37(11)	7(11)	-46(10)
C(41)	169(14)	169(16)	134(13)	-33(11)	9(10)	-46(11)
C(42)	163(13)	158(14)	128(14)	-27(10)	13(10)	-41(11)
C(43)	164(14)	170(16)	135(13)	-27(11)	16(10)	-46(12)
C(44)	152(13)	159(14)	119(15)	-19(10)	15(11)	-35(11)
C(45)	153(16)	173(13)	120(12)	-23(10)	18(11)	-34(10)
C(46)	138(16)	171(13)	110(12)	-21(10)	20(10)	-29(9)
C(47)	138(12)	161(13)	101(12)	-22(9)	17(10)	-21(9)
C(48)	143(12)	158(14)	102(11)	-23(10)	19(9)	-18(10)
C(49)	140(11)	141(14)	91(11)	-26(9)	13(8)	-16(10)
C(50)	153(12)	126(16)	101(10)	-20(10)	0(8)	-27(10)

C(51)	154(13)	150(14)	102(11)	-28(11)	-3(9)	-24(9)
C(52)	150(14)	151(12)	104(11)	-29(9)	-8(10)	-23(9)
C(53)	147(16)	162(12)	109(12)	-34(10)	3(11)	-36(9)
C(54)	145(15)	160(12)	106(14)	-36(9)	13(12)	-34(9)
C(55)	139(13)	141(11)	94(14)	-33(9)	18(10)	-28(9)
C(56)	148(12)	148(12)	103(16)	-26(9)	15(9)	-26(10)
C(57)	145(13)	148(12)	114(17)	-24(9)	16(10)	-29(10)
C(58)	129(11)	145(11)	85(13)	-18(8)	13(9)	-25(8)
C(59)	125(11)	132(11)	80(9)	-25(8)	13(7)	-24(8)
C(60)	125(12)	138(11)	82(9)	-28(8)	14(8)	-25(8)
C(61)	116(12)	116(11)	76(8)	-16(8)	12(7)	-17(7)
C(62)	102(16)	100(12)	71(8)	-13(11)	13(8)	-23(7)
O(63)	107(17)	102(12)	84(13)	-12(11)	0(11)	-29(9)
O(64)	94(14)	91(12)	63(8)	-18(10)	11(8)	-18(8)
C(65)	117(17)	99(13)	68(9)	-51(13)	-2(9)	-17(8)
C(66)	120(17)	99(13)	68(9)	-55(13)	-4(9)	-14(9)
N(67)	160(20)	100(13)	88(14)	-56(13)	-29(13)	-14(9)
C(68)	111(15)	112(11)	63(14)	-20(9)	10(11)	-12(9)
O(69)	129(15)	115(18)	150(30)	-2(13)	-34(17)	-62(18)
O(70)	134(17)	118(15)	110(20)	-19(11)	-22(14)	-23(13)
C(71)	180(30)	150(20)	170(30)	15(19)	-60(20)	-70(20)
C(72)	190(30)	180(40)	170(30)	0(20)	-50(20)	-80(30)
N(73)	190(30)	80(30)	140(30)	-30(20)	-50(20)	20(20)

The anisotropic displacement factor exponent takes the form: $-2\pi^2[h^2a^{*2}U_{11} + ... + 2hka^*b^*U_{12}]$.

Table S4. Bond lengths [Å] for $(C_{60}\text{-}2NH_3)Pb_2I_6$ at 296.15 K with estimated standard deviations in parentheses.

Label	**Distances**
Pb(1)-I(1)	3.149(3)
Pb(1)-I(2)	3.204(3)
Pb(1)-I(4)	3.320(2)
Pb(1)-I(5)	3.245(3)
Pb(1)-I(6)	3.011(3)
Pb(2)-I(1)	3.174(3)
Pb(2)-I(2)#1	3.311(3)
Pb(2)-I(3)	3.268(2)
Pb(2)-I(3)#1	3.277(2)
Pb(2)-I(4)#2	3.163(2)
Pb(2)-I(5)#3	3.128(3)
C(1)-C(2)	1.36(3)
C(1)-C(6)	1.52(3)
C(1)-C(20)	1.43(3)
C(2)-C(3)	1.48(3)
C(2)-C(17)	1.30(3)
C(3)-C(4)	1.36(3)
C(3)-C(15)	1.51(3)
C(4)-C(5)	1.52(3)
C(4)-C(12)	1.39(3)
C(5)-C(6)	1.41(3)
C(5)-C(10)	1.51(3)
C(6)-C(7)	1.37(3)
C(7)-C(8)	1.43(3)
C(7)-C(21)	1.49(3)

C(8)-C(9)	1.49(3)
C(8)-C(38)	1.38(3)
C(9)-C(10)	1.33(3)
C(9)-C(36)	1.36(3)
C(10)-C(11)	1.53(3)
C(11)-C(12)	1.46(3)
C(11)-C(34)	1.32(3)
C(12)-C(13)	1.31(3)
C(13)-C(14)	1.55(3)
C(13)-C(32)	1.25(3)

Symmetry transformations used to generate equivalent atoms:

(1) -x-1,-y+2,-z (2) x,y+1,z (3) -x-2,-y+2,-z (4) x,y-1,z

Table S5. Bond angles [°] for $(C_{60}\text{-}2NH_3)Pb_2I_6$ at 296.15 K with estimated standard deviations in parentheses.

Label	**Angles**
I(1)-Pb(1)-I(2)	90.63(10)
I(1)-Pb(1)-I(4)	170.95(8)
I(1)-Pb(1)-I(5)	92.31(11)
I(2)-Pb(1)-I(4)	85.16(7)
I(2)-Pb(1)-I(5)	171.93(9)
I(5)-Pb(1)-I(4)	90.85(8)
I(6)-Pb(1)-I(1)	92.16(9)
I(6)-Pb(1)-I(2)	95.60(9)
I(6)-Pb(1)-I(4)	96.22(8)
I(6)-Pb(1)-I(5)	91.80(10)
I(1)-Pb(2)-I(2)#1	171.71(7)
I(1)-Pb(2)-I(3)#1	96.11(10)
I(1)-Pb(2)-I(3)	87.91(6)
I(3)-Pb(2)-I(2)#1	84.04(6)
I(3)#1-Pb(2)-I(2)#1	85.40(6)
I(3)-Pb(2)-I(3)#1	86.58(6)
I(4)#2-Pb(2)-I(1)	91.06(7)
I(4)#2-Pb(2)-I(2)#1	97.14(7)
I(4)#2-Pb(2)-I(3)#1	87.97(6)
I(4)#2-Pb(2)-I(3)	174.31(7)
I(5)#3-Pb(2)-I(1)	93.94(11)
I(5)#3-Pb(2)-I(2)#1	84.26(8)
I(5)#3-Pb(2)-I(3)#1	169.56(8)
I(5)#3-Pb(2)-I(3)	90.96(7)
I(5)#3-Pb(2)-I(4)#2	94.69(8)

Pb(1)-I(1)-Pb(2)	97.14(8)
Pb(1)-I(2)-Pb(2)#1	96.99(7)
Pb(2)-I(3)-Pb(2)#1	93.42(5)
Pb(2)#4-I(4)-Pb(1)	167.54(9)
Pb(2)#3-I(5)-Pb(1)	170.95(13)
C(2)-C(1)-C(6)	121(3)
C(2)-C(1)-C(20)	120(4)
C(20)-C(1)-C(6)	108(3)
C(1)-C(2)-C(3)	118(3)
C(17)-C(2)-C(1)	122(4)
C(17)-C(2)-C(3)	111(3)
C(2)-C(3)-C(15)	111(3)
C(4)-C(3)-C(2)	127(3)
C(4)-C(3)-C(15)	114(3)
C(3)-C(4)-C(5)	114(3)
C(3)-C(4)-C(12)	125(4)
C(12)-C(4)-C(5)	109(3)
C(6)-C(5)-C(4)	122(3)
C(6)-C(5)-C(10)	115(3)
C(10)-C(5)-C(4)	109(3)
C(5)-C(6)-C(1)	118(3)
C(7)-C(6)-C(1)	103(3)
C(7)-C(6)-C(5)	127(3)
C(6)-C(7)-C(8)	118(3)

Symmetry transformations used to generate equivalent atoms:

(1) -x-1,-y+2,-z (2) x,y+1,z (3) -x-2,-y+2,-z (4) x,y-1,z

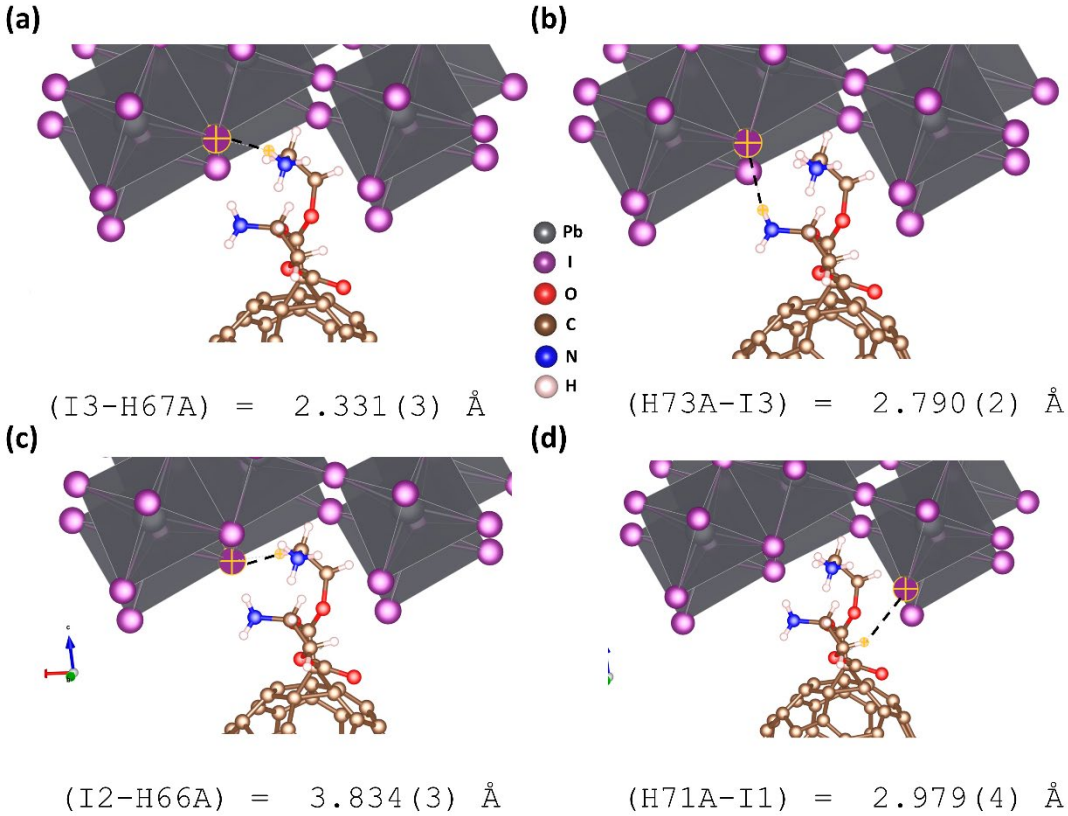

Figure S8. (a-d) Part of the crystal structures of $(C_{60}\text{-}2NH_3)Pb_2I_6$, showcasing the different types of hydrogen bonds along with corresponding distances among the organic counter-cation and the iodide ions of the inorganic layer.

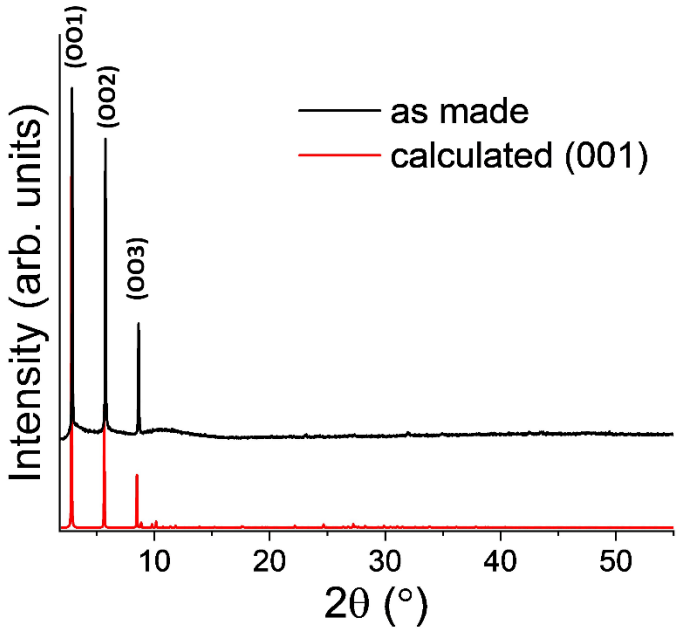

Figure S9. Comparison of the PXRD patterns for the as-made $(C_{60}\text{-}2NH_3)Pb_2I_6$ crystals to the calculated pattern based on the solved single-crystal structure, including preferred orientation (001).

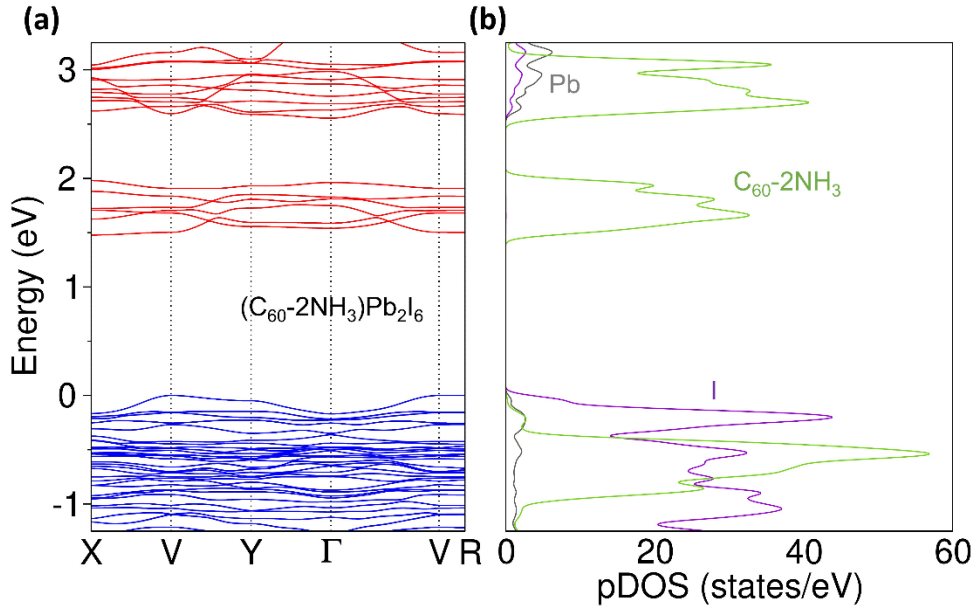

Figure S10. (a) Calculated band structure of $(C_{60}\text{-}2NH_3)Pb_2I_6$ and (b) density of states projected on Pb (green), I (violet), and $C_{60}\text{-}NH_3$ states using HSE06 correction for the band gaps (*vide supra*).

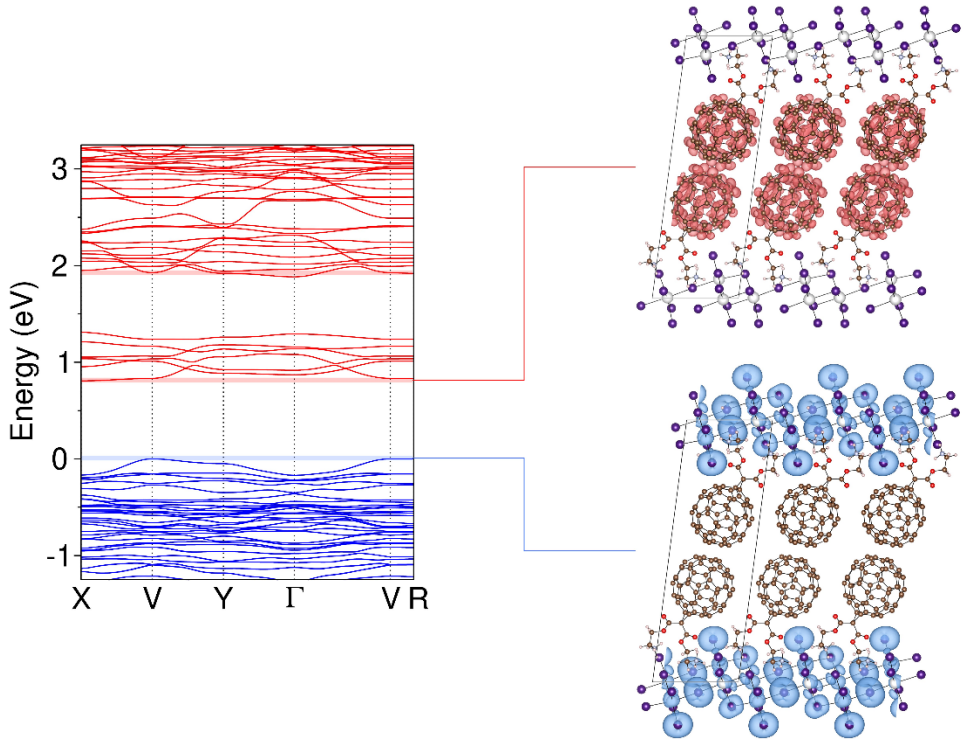

Figure S11. Partial charge density taken at the valence band maximum (blue, bottom), at the conduction band minimum (red, top).

Table S6. Bandgaps in eV computed for $(C_{60}\text{-}2NH_3)Pb_2I_6$, $Cs_2Pb_2I_6$, and $C_{60}\text{-}2CH_3$ using the VASP code with GGA and the HSE06 hybrid functional, and with SIESTA using a GGA functional. In all cases, the spin-orbit coupling is included in the calculations. The last column gives the SIESTA gaps corrected by the HSE06 correction found in VASP calculations.

	VASP		SIESTA	
	GGA	HSE06	GGA	GGA+Shift
$(C_{60}\text{-}2NH_3)Pb_2I_6$ Gap V→X	0.96	1.63	0.81	1.48
$Cs_2Pb_2I_6$ Gap V→V	1.76	2.35	1.86	2.45
$C_{60}\text{-}(CH_3)_2$ Gap X→X	1.14	1.67	1.17	1.70

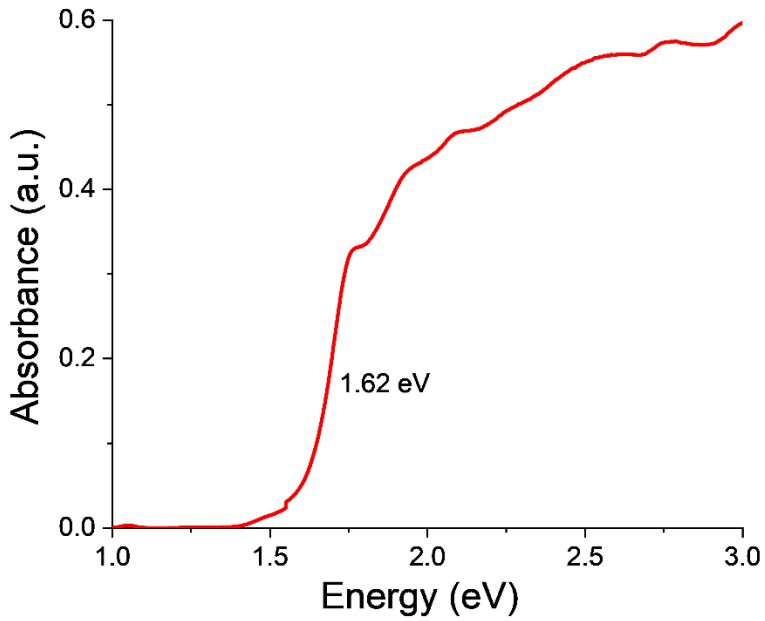

Figure S12. UV-VIS absorption spectrum of $(C_{60}\text{-}2NH_3)Pb_2I_6$.

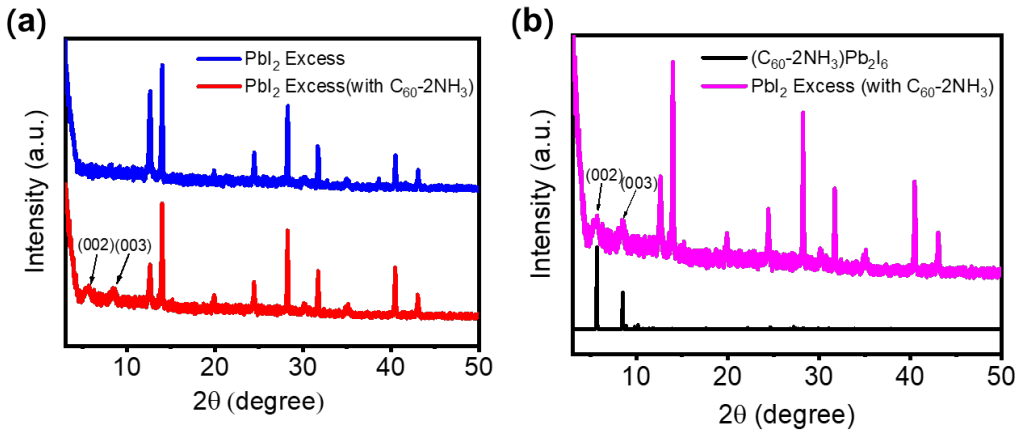

Figure S13. (a) PXRD patterns of PbI_2-excessive perovskite films without and with C_{60}-$2NH_3$ post-treatment. (b) PXRD patterns of $(C_{60}\text{-}2NH_3)Pb_2I_6$ single crystal powders and PbI_2-excessive perovskite films modified with C_{60}-$2NH_3$. The appearance of 2 diffraction peaks at 5.6° and 8.5°, correspond to the (002) and (003) planes of 2D $(C_{60}\text{-}2NH_3)Pb_2I_6$. This finding validates that a 2D layer can indeed be formed on the 3D perovskite layer.

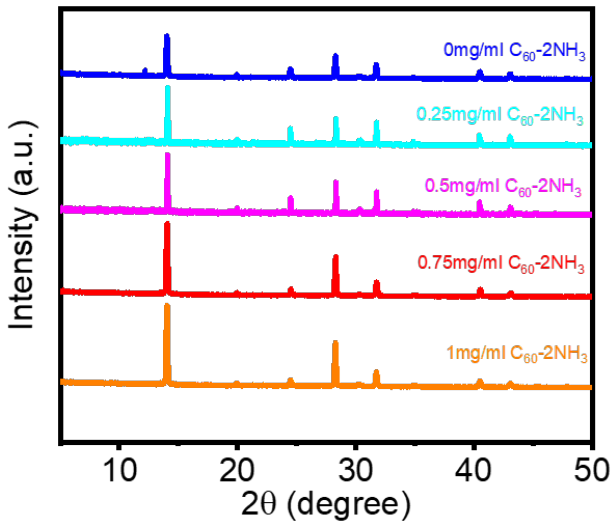

Figure S14. PXRD patterns of perovskite films post-treated with various concentrations of C_{60}-$2NH_3$.

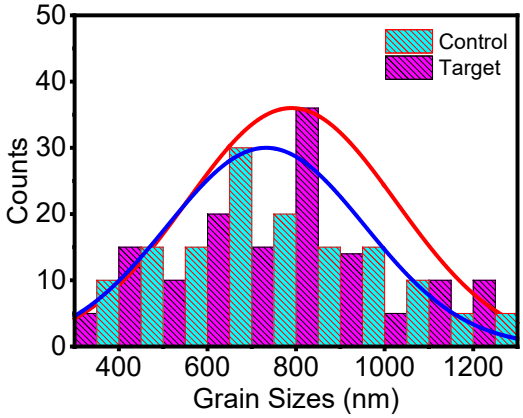

Figure S15. Statistical graph of grain size of control and target perovskite films.

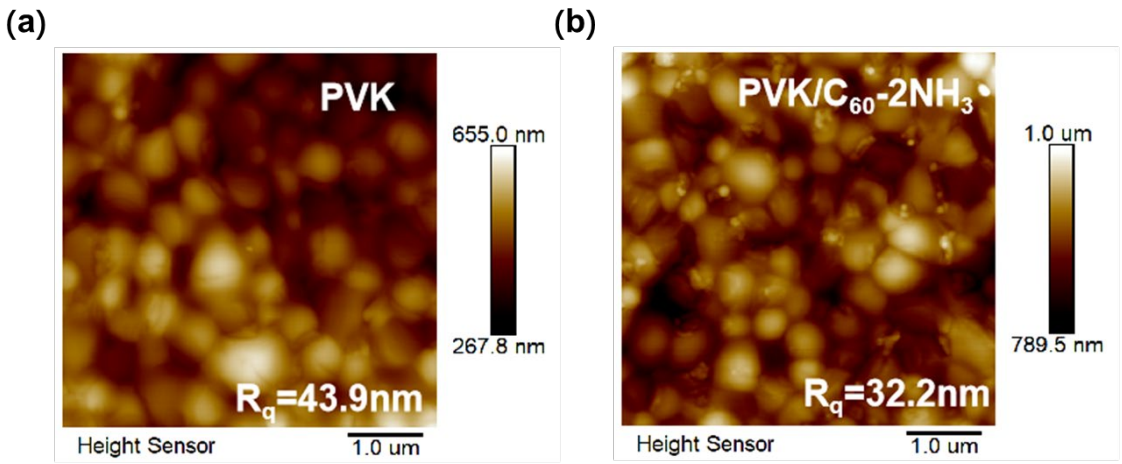

Figure S16. AFM images of perovskite films with and without C_{60}-2NH_3 post-treatment.

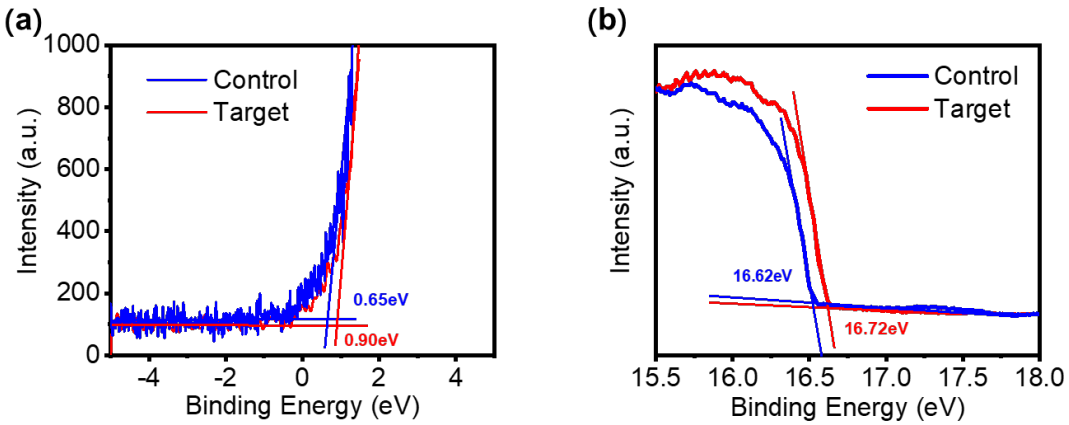

Figure S17. (a, b) UPS spectra of control and target films.

Estimation of E_f from KPFM data.

The data obtained from KPFM measurements was contact potential difference (CPD, i.e., the mean value here). When DC voltage (V_{dc}) was applied to a sample, the relationship between the measured CPD and the work function (Φ) of the sample was $V_{CPD} = (\Phi_{sample} - \Phi_{tip})/e$. Accordingly, we can list the following equations:

$$V_{CPD\text{-}HOPG} = (\Phi_{HOPG} - \Phi_{tip}) / e = -0.047 \text{ V},$$

$$V_{CPD\text{-}Control} = (\Phi_{Control} - \Phi_{tip}) / e = 0.064 \text{ V},$$

$$V_{CPD\text{-}Target} = (\Phi_{Target} - \Phi_{tip}) / e = -0.015 \text{ V},$$

then we obtained $\Phi_{Control} - \Phi_{HOPG} = 0.111$ eV, and $\Phi_{Target} - \Phi_{HOPG} = 0.032$ eV. Since $\Phi_{HOPG} = 4.500$ eV, $\Phi_{Control} = 4.611$ eV and $\Phi_{Target} = 4.532$ eV could be calculated.

Table S7. The mean surface potentials of the control and target films and their calculated E_f.

	Mean (V)	E_f (eV)
Control	0.064	-4.61
Target	-0.015	-4.53

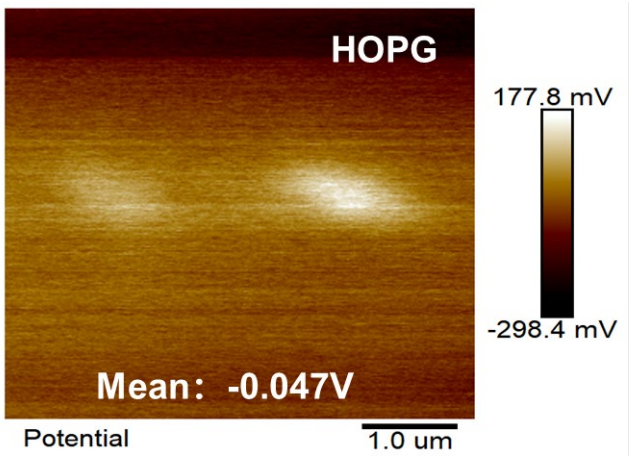

Figure S18. KPFM image of a highly oriented pyrolytic graphite (HOPG).

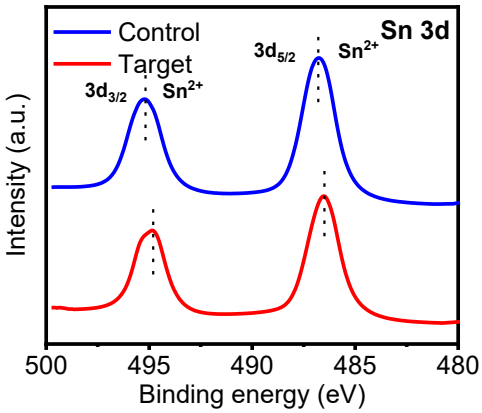

Figure S19. Sn 3d XPS spectra of perovskite films with and without C_{60}-2NH_3 post-treatment.

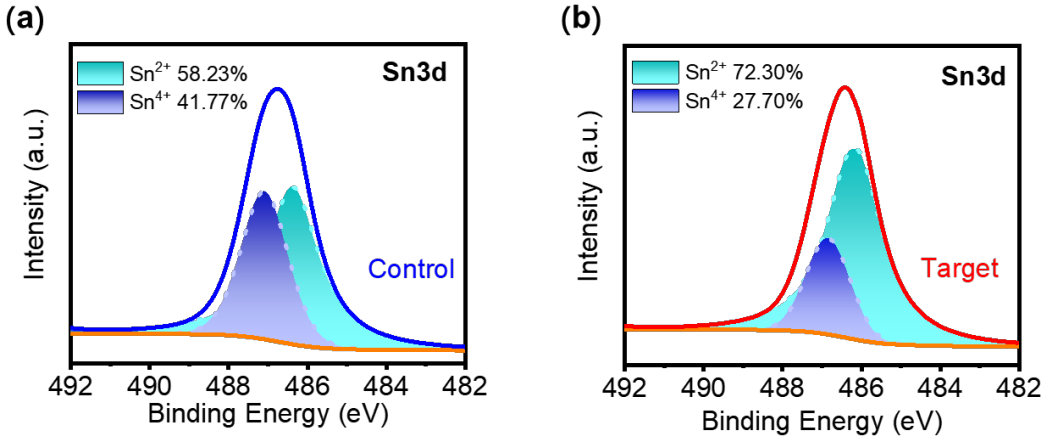

Figure S20. Sn 3d XPS spectra of perovskite films without (a) and with C_{60}-2NH_3 (b) post-treatment (area of Sn^{2+} and Sn^{4+}).

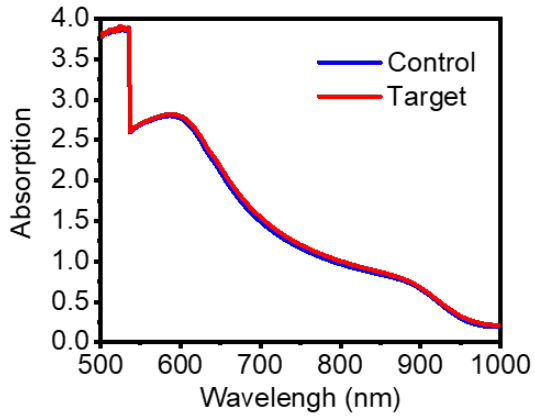

Figure S21. UV-VIS absorption spectra of perovskite films with and without C_{60}-2NH_3 post-treatment.

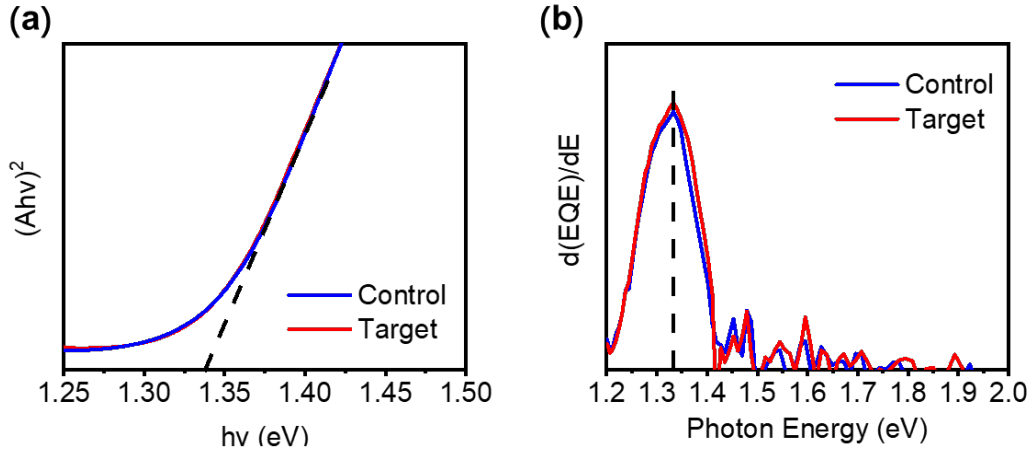

Figure S22. (a) Tauc plots of $FA_{0.6}MA_{0.4}Pb_{0.7}Sn_{0.3}I_3$ films with and without C_{60}-2NH_3 post-treatment. (b) Derived bandgaps from the peak of the first derivation of EQE curves.

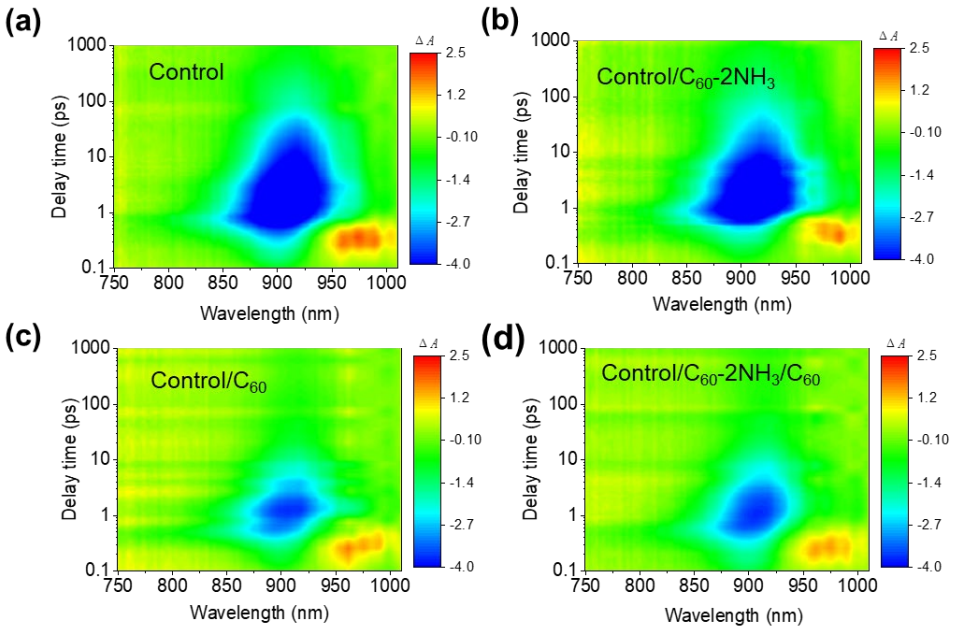

Figure S23. 2D color plots of TA spectra on control perovskite films (a), perovskite/ C_{60}-$2NH_3$ films (b), control perovskite/C_{60} films (c) and perovskite/ C_{60}-$2NH_3$/C_{60} films (d).

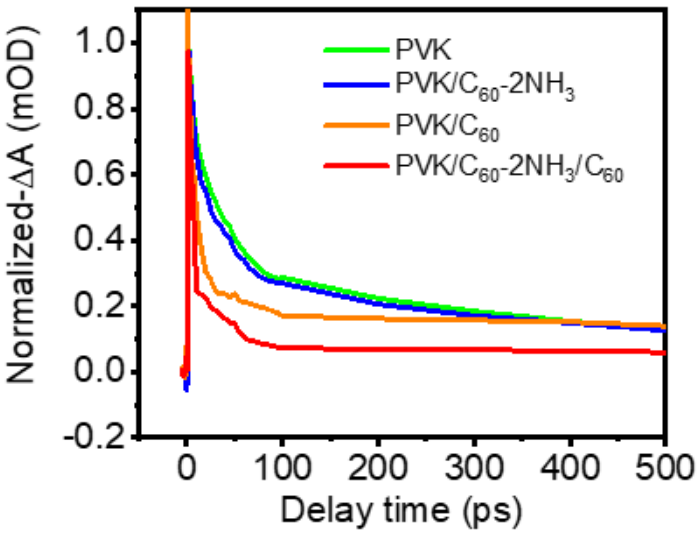

Figure S24. Corresponding normalized decay kinetic curves at 925 nm.

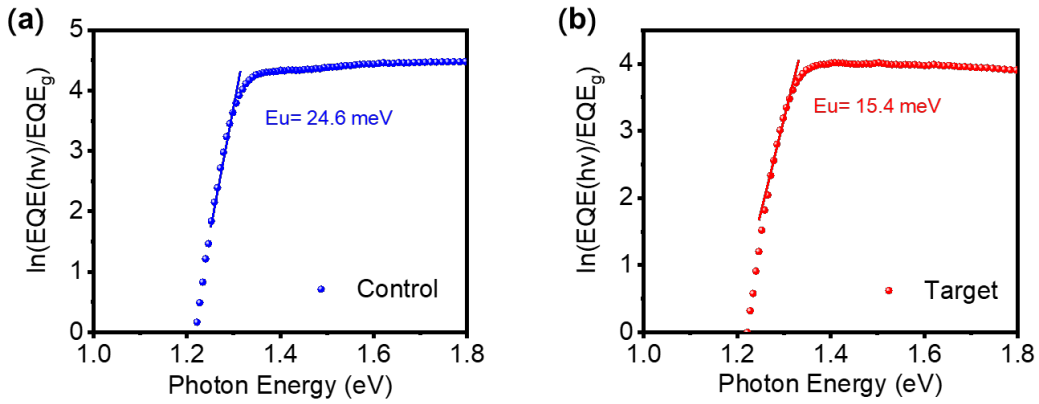

Figure S25. *E*u calculation using the EQE spectra for perovskite films without (a) and with (b) C_{60}-$2NH_3$ post-treatment.

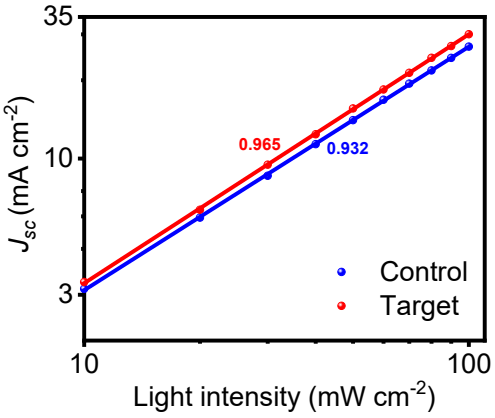

Figure S26. Light intensity-dependent J_{SC} changes and slopes of the linear fittings.

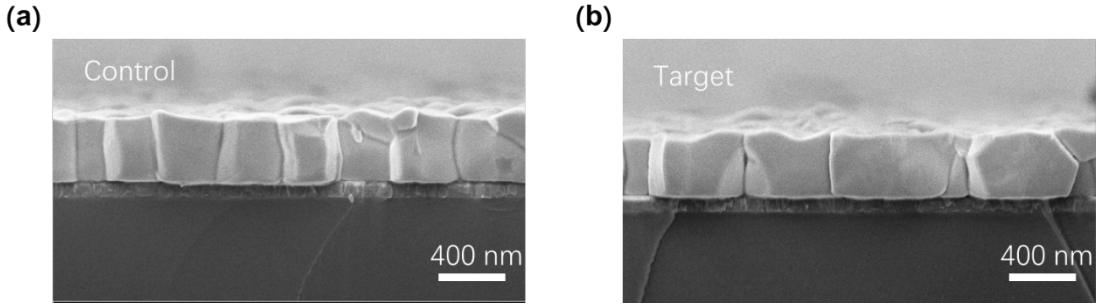

Figure S27. Cross-sectional SEM images of perovskite films without (a) and with (b) C_{60}-$2NH_3$ post-treatment.

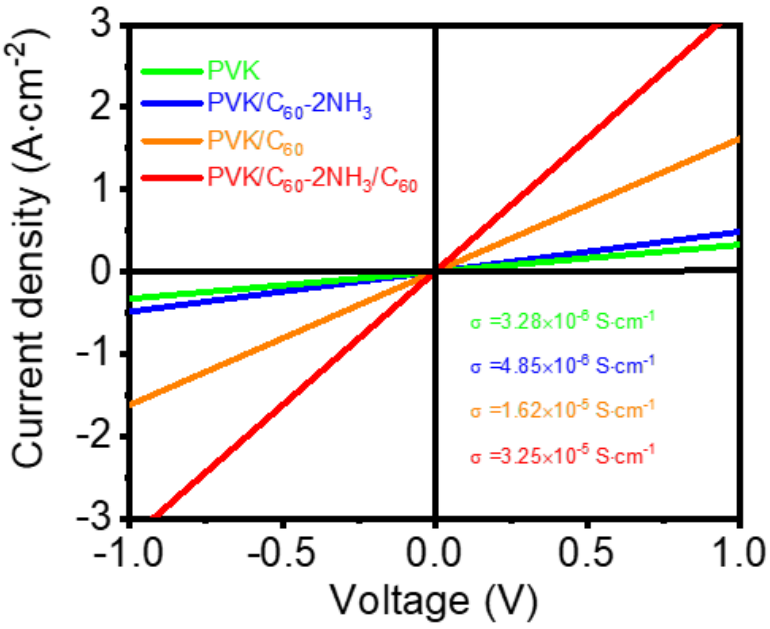

Figure S28. Electrical conductivity of control perovskite films, perovskite/ C_{60}-$2NH_3$ films, control perovskite/C_{60} films, and perovskite/ C_{60}-$2NH_3$/ C_{60} films.

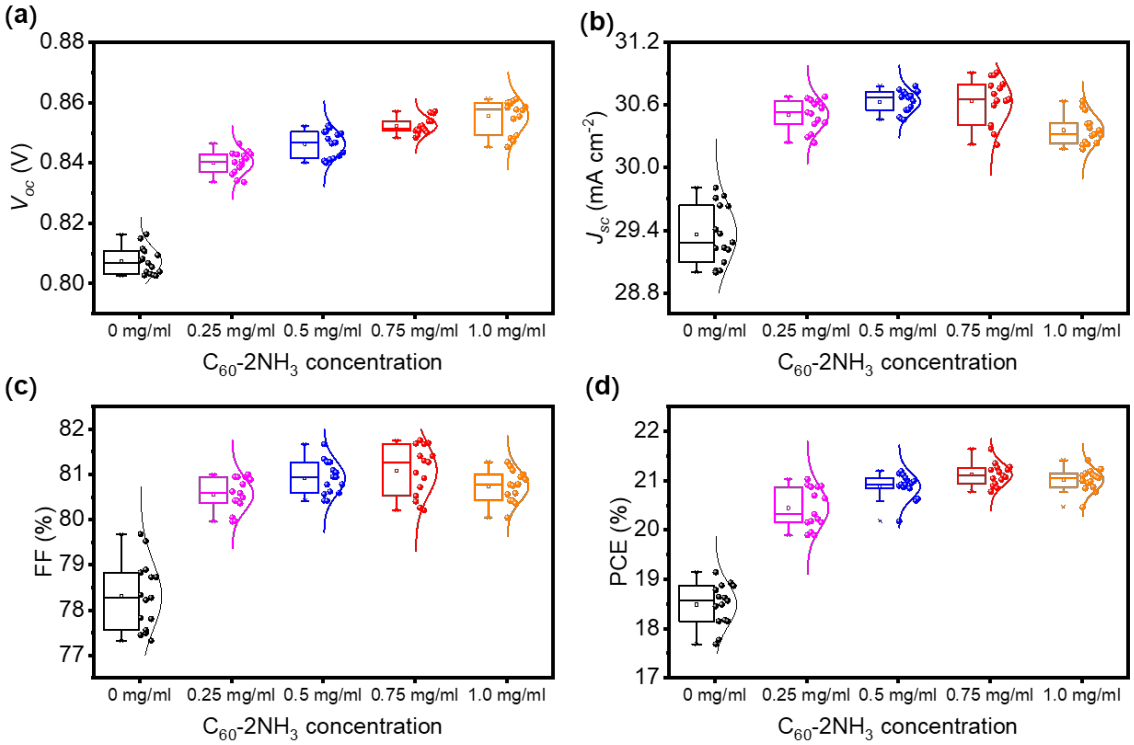

Figure S29. Photovoltaic performance of PSCs with various C_{60}-$2NH_3$ concentrations.

Table S8. Average photovoltaic parameters of PSCs post-treated with various C_{60}-2NH_3 concentrations.

	V_{OC} (V)	J_{SC} (mA cm^{-2})	FF %	PCE %
0mg/ml	0.79±0.01	29.52±0.45	79.62±0.86	18.62±0.86
0.25mg/ml	0.83±0.01	30.45±0.23	80.52±0.43	20.43±0.64
0.5mg/ml	0.84±0.01	30.62±0.18	80.78±0.82	20.76±0.50
0.75mg/ml	0.85±0.01	30.65±0.32	81.23±0.41	21.16±0.48
1mg/ml	0.85±0.01	30.34±0.28	80.69±0.70	20.82±0.45

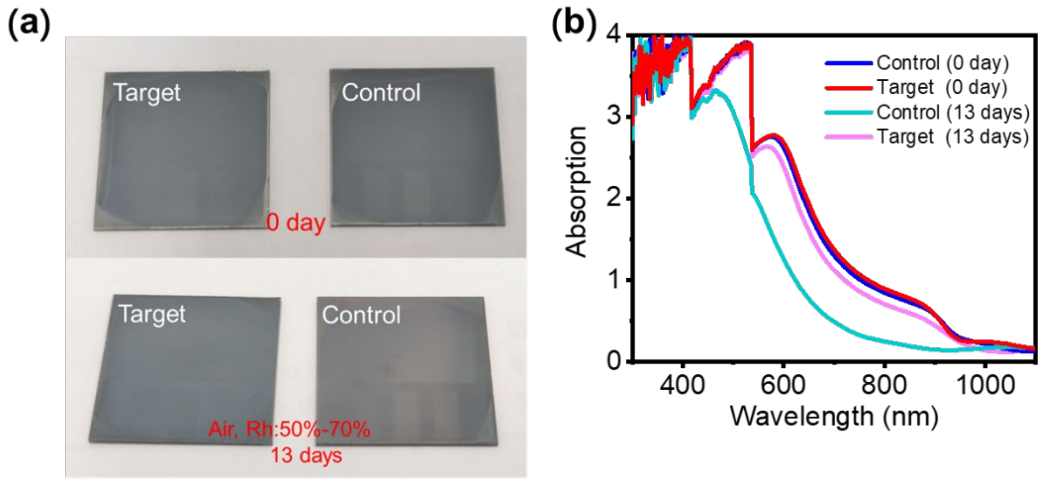

Figure S30. (a) Photographs and (b) UV-VIS absorption spectra of control and target perovskite films after 0 and 13 days of storage in ambient air.

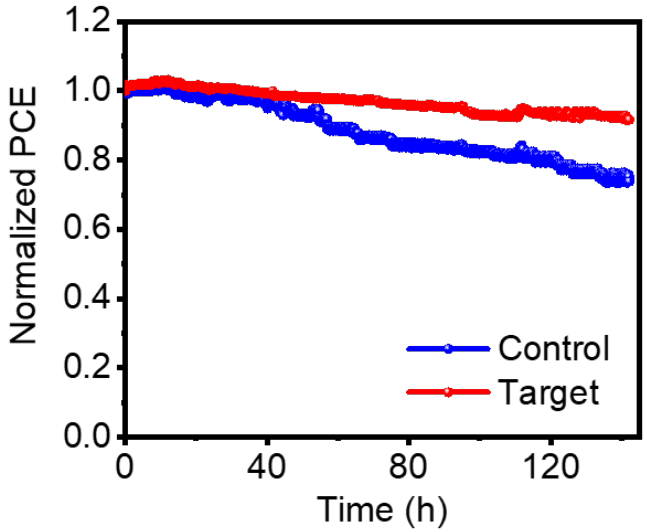

Figure S31. (a) MPP tracking of unencapsulated control and target devices at around 55°C without a cooling system.

References

1. Bruker, APEX4. Bruker AXS LLC, Madison, Wisconsin, USA., **2022**.
2. Bruker, SAINT. Bruker AXS LLC, Madison, Wisconsin, USA., **2022**.
3. Krause, L.; Herbst-Irmer, R.; Sheldrick, G. M.; Stalke, D., Comparison of Silver and Molybdenum Microfocus X-ray Sources for Single-crystal Structure Determination, *J Appl Crystallogr* **2015,** *48*, 3-10.
4. Sheldrick, G., SHELXT - Integrated Space-group and Crystal-structure Determination, *Acta Crystallogr. Sect. A* **2015,** *71*, 3-8.
5. Sheldrick, G., Crystal Structure Refinement with SHELXL, *Acta Crystallogr. Sect. C* **2015,** *71*, 3-8.
6. Dolomanov, O. V.; Bourhis, L. J.; Gildea, R. J.; Howard, J. A. K.; Puschmann, H., OLEX2: a Complete Structure Solution, Refinement and Analysis Program, *J. Appl. Crystallogr.* **2009,** *42*, 339-341.
7. Spek, A., Single-crystal Structure Validation with the Program PLATON, *J. Appl. Crystallogr.* **2003,** *36*, 7-13.
8. Gate, L. F., Comparison of the Photon Diffusion Model and Kubelka-Munk Equation with the Exact Solution of the Radiative Transport Equation, *Appl. Opt.* **1974,** *13*, 236-238.
9. Soler, J. M.; Artacho, E.; Gale, J. D.; García, A.; Junquera, J.; Ordejón, P.; Sánchez-Portal, D., The SIESTA method forab initioorder-Nmaterials simulation, *J. Phys.: Condens. Matter* **2002,** *14*, 2745-2779.
10. García, A.; Papior, N.; Akhtar, A.; Artacho, E.; Blum, V.; Bosoni, E.; Brandimarte, P.; Brandbyge, M.; Cerdá, J. I.; Corsetti, F.; Cuadrado, R.; Dikan, V.; Ferrer, J.; Gale, J.; García-Fernández, P.; García-Suárez, V. M.; García, S.; Huhs, G.; Illera, S.; Korytár, R.; Koval, P.; Lebedeva, I.; Lin, L.; López-Tarifa, P.; Mayo, S. G.; Mohr, S.; Ordejón, P.; Postnikov, A.; Pouillon, Y.; Pruneda, M.; Robles, R.; Sánchez-Portal, D.; Soler, J. M.; Ullah, R.; Yu, V. W.-z.; Junquera, J., Siesta: Recent developments and applications, *J. Chem. Phys.* **2020,** *152*.
11. Dion, M.; Rydberg, H.; Schröder, E.; Langreth, D. C.; Lundqvist, B. I., Van der Waals Density Functional for General Geometries, *Phys. Rev. Lett.* **2004,** *92*, 246401.
12. Cooper, V. R., Van der Waals density functional: An appropriate exchange functional, *Phys. Rev. B* **2010,** *81*, 161104.
13. Zhang, Y.; Yang, W., Comment on ``Generalized Gradient Approximation Made Simple'', *Phys. Rev. Lett.* **1998,** *80*, 890-890.
14. Cuadrado, R.; Cerdá, J. I., Fully relativistic pseudopotential formalism under an atomic orbital basis: spin–orbit splittings and magnetic anisotropies, *J. Phys.: Condens. Matter* **2012,** *24*, 086005.
15. Troullier, N.; Martins, J. L., Efficient pseudopotentials for plane-wave calculations, *Phys. Rev. B* **1991,** *43*, 1993-2006.
16. Artacho, E.; Sánchez-Portal, D.; Ordejón, P.; García, A.; Soler, J. M., Linear-Scaling ab-initio Calculations for Large and Complex Systems, *physica status solidi (b)* **1999,** *215*, 809-817.
17. Kresse, G.; Furthmüller, J., Efficient iterative schemes for ab initio total-energy calculations using a plane-wave basis set, *Phys. Rev. B* **1996,** *54*, 11169-11186.
18. Kresse, G.; Joubert, D., From ultrasoft pseudopotentials to the projector augmented-wave method, *Phys. Rev. B* **1999,** *59*, 1758-1775.
19. Even, J.; Pedesseau, L.; Kepenekian, M., Electronic surface states and dielectric self-energy profiles in colloidal nanoscale platelets of CdSe, *Phys. Chem. Chem. Phys.* **2014,** *16*, 25182-25190.
20. Sapori, D.; Kepenekian, M.; Pedesseau, L.; Katan, C.; Even, J., Quantum confinement and dielectric profiles of colloidal nanoplatelets of halide inorganic and hybrid organic–inorganic perovskites, *Nanoscale* **2016,** *8*, 6369-6378.